Politecnico di Torno

Corso di Laurea Magistrale in Tunnelling
A.a. 2023/2024
Sessione di Laurea Mese Anno

Rock TBM production forecast and model comparison

Relatori:

Daniele Peila

Carmine Todaro

Candidati:

Jamie Brincat Brockdorff

Abstract

The scope was to create an excel file program capable of using the major prediction models to determine TBM cutter wear. Results were then tested against hand calculations and graphical methods to build a comprehensive database capable of offering insight into the efficacy of the prediction models and how they compare with each other.

Various sources of literature were consulted to derive the necessary equations, parameters and graphs to develop a rigorous comparison of results.

1. Introduction

Tunnel excavation is an age old procedure, with the modern mechanised conception emerging in the 1800s. Isambard Brunel was the first to develop and use a tunnelling shield which was used to make the excavation of the Thames Tunnel (1825) safer. This idea was adapted 20 years later, when an actual boring machine was built to partially excavate the Frejus Rail Tunnel.

In 1853 in the United States, Charles Wilson developed his own boring machine which was the first to utilise cutting discs. This machine was used in Northwest Massachusetts to construct the Hoosac Tunnel. In the following years, various methods and designs were subsequently developed, but real improvements were made in the early 1900s all the way up to the 2000s. The Robbins Company was one of the earliest industry leaders, giving themselves a name when they built a 14.4 meter diameter TBM for the Niagara Tunnel Project.

As knowledge in the field steadily grew, and new materials and manufacturing processes became available, several new types of TBMs came into existence. The machines of today are now able to excavate in most rock and soil types, employing various design principals depending on strata. Additionally, these modern TBMs also feature shields, gripper systems, slurry capabilities, and the ability to resist earth pressure which are all aspects dependant on rock or soft ground conditions.

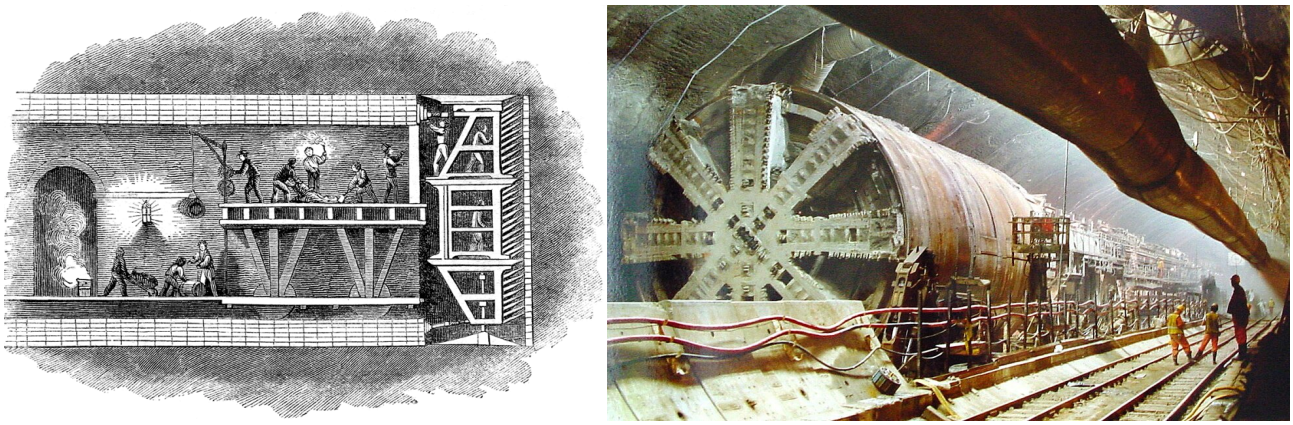

Figure 1: Left - Brunel's tunnelling shield used to excavate the Thames Tunnel 1825, Illustrated London News. Right - One of TBMs used in the Channel Tunnel between England and France

2. Mechanised tunnelling with Tunnel Boring Machines in rock formations

Rock TBMs can be classified into various types, each with their own unique ways of dealing with tunnel excavation and construction. The choice on what type of machine is to be used is largely dependant on the geological conditions, which in turn has an effect on various parameters such as the advancement rate, and cutter wear. The machines must also be custom built for the desired project and it is extremely rare that they may be reused in different conditions. Each TBM is a specialised tool for a particular set of conditions. That being said, some machine types such as the Double-shield, are capable of handling changes in the geology.

In terms of the functional and technical characteristics, the classification of machines used for full face excavation can be split between Open and Shielded. As previously mentioned, each machine is custom designed based on site constraints, and as a result, will have different sizes and characteristics and is perfectly illustrated in Figure 2 from Volume 2 of Handbook on Tunnels and Underground Works:

			Rock TBM - Suitability and Application Ranges						
Dimension range		Tunnel Equivalent Diameter (m)	<2.5	2.5-5.0	5.0-8.0	8.0-10.0	10.0-12.5	12.5-15.0	>15.0
		Typical purposes	Services, Water facilities			Rail&Metro, Road, Hydro&water Multipurpose			Road Multipurpose
Open Mode TBM	Support type		Temporary supports according to design criteria						
	Geological-geotechnical constraints	Rock							
		Soils							
		Mixed conditions							
		Under water head							
		Face support required							
		Immediate tubbing required							
	Geometrical /site conditions constraints	Long&Deep tunnel							
		Shallow tunnel							
		Urban tunnel							
	Performance ranges	Average daily A.R. (m)	20-40	20-40	15-35	10-30	5-25	*	*
		Procurement - FAT (mths)	7-10	7-10	9-12	9-12	12	*	*
		Manpower (men/shift)	8	8	8-10	8-10	8-10	*	*
		Cutterhead - Power (kW)	1.100-1.500	1.700-2.000	2.500-3.500	4.000-4.500	4.500-5.000	≥5.000	*
		Cutterhead - Torque (kNm)	1.000-1.250	1.000-1.250	2.000-8.000	10.000-20.000	15.000-25.000	≥20.000	*
		Nominal Thrust (kN)	8.000-10.000	8.000-10.000	10.000-15.000	15.000-18.000	18.000-20.000	≥20.000	*
Single Shield TBM	Support type		Segmental lining						
	Geological-geotechnical constraints	Rock							
		Soils							
		Mixed conditions							
		Under water head							
		Face support required							
		Immediate tubbing required							
	Geometrical /site conditions constraints	Long&Deep tunnel							
		Shallow tunnel							
		Urban tunnel							
	Performance ranges	Average daily A.R. (m)	20-40	20-40	15-35	10-30	5-25	5-10	*
		Procurement - FAT (mths)	10-12	10-12	12-14	12-14	12-14	*	*
		Manpower (men/shift)	10	10	10-12	10-12	10-12	*	*
		Cutterhead - Power (kW)	1.000-1.300	1.300-1.500	2.500-3.500	4.000-5.000	5.000-7.000	*	*
		Cutterhead - Torque (kNm)	1.000-1.500	1.500-2.000	4.500-6.000	15.000-25.000	25.000-30.000	*	*
		Nominal Thrust (kN)	4.500-5.500	15.000-20.000	25.000-35.000	35.000-50.000	50.000-70.000	*	*
Double Shield TBM	Support type		Segmental lining OR temporary supports according to design criteria						
	Geological-geotechnical constraints	Rock							
		Soils							
		Mixed conditions							
		Under water head							
		Face support required							
		Immediate tubbing required							
	Geometrical /site conditions constraints	Long&Deep tunnel							
		Shallow tunnel							
		Urban tunnel							
	Performance ranges	Average daily A.R. (m)	20-40	20-40	15-35	10-30	5-25	5-10	*
		Procurement - FAT (mths)	10-12	10-12	12-14	12-14	*	*	*
		Manpower (men/shift)	10	10	10-12	10-12	*	*	*
		Cutterhead - Power (kW)	1.000-1.300	1.300-1.500	2.500-3.500	4000-5000	*	*	*
		Cutterhead - Torque (kNm)	1.000-1.500	1.500-2.000	4.500-6.000	15000-25000	*	*	*
		Nominal Thrust (kN)	4.500-5.500	15.000-20.000	25000-35000	35000-50000	*	*	*

Figure 2: Machine performance and suitability in various rock types. Adapted from P. Grasso et al. (2023), figure 2.22

2.1 Open TBM

As these TBMs are “open”, they are best suited for favourable rock conditions. This can be defined as a rock quality which has a good stand up time and therefor does not need major support up until the point of collapse. In cases where there may be some degree of instability, some basic temporary supports such as rock bolting or shotcrete should be implemented between 3 and 30 meters away from the cutterhead.

Open TBMs exist in two forms, and their use is justified based on the desired anchoring system. Those with a single anchoring system are known as “Main Beam” type and those with a double anchoring system are commonly known as “Kelly Style” TBMs. The decision to use a single or double anchoring system is usually taken depending on the excavation diameter.

The Main Beam types will have one pair of gripper pads, whilst the Kelly Style will use two pairs. All the other mechanical components are usually the same, with the main ones being the cutterhead along with its cutting discs and the associated system for mucking, thrust jacks, hydraulics, electronics, and a safety shield.

In both systems, the machine is pushed forward by thrust generated by hydraulic cylinders and is held in place by the gripper systems which provide contrast forces. As the head is being pushed forward, it also rotates, crushes the rock ahead and collects the debris in buckets built into the machine face. From there, the crushed rock is carried out via the mucking system. When jacks reach full extension, the grippers are readjusted into a forward position and the process repeats itself.

In terms of directional changes, the single gripper machine is not fixed axially along the tunnel axis due to the weight of the cutterhead, and thus the machine is able to adjust its direction during the actual excavation process. In the Kelly Style, directional change is only possible before the next advancement step as the double anchoring system prevents any change in direction during the excavation portion of the movement. The machine can also be stopped and then realigned.

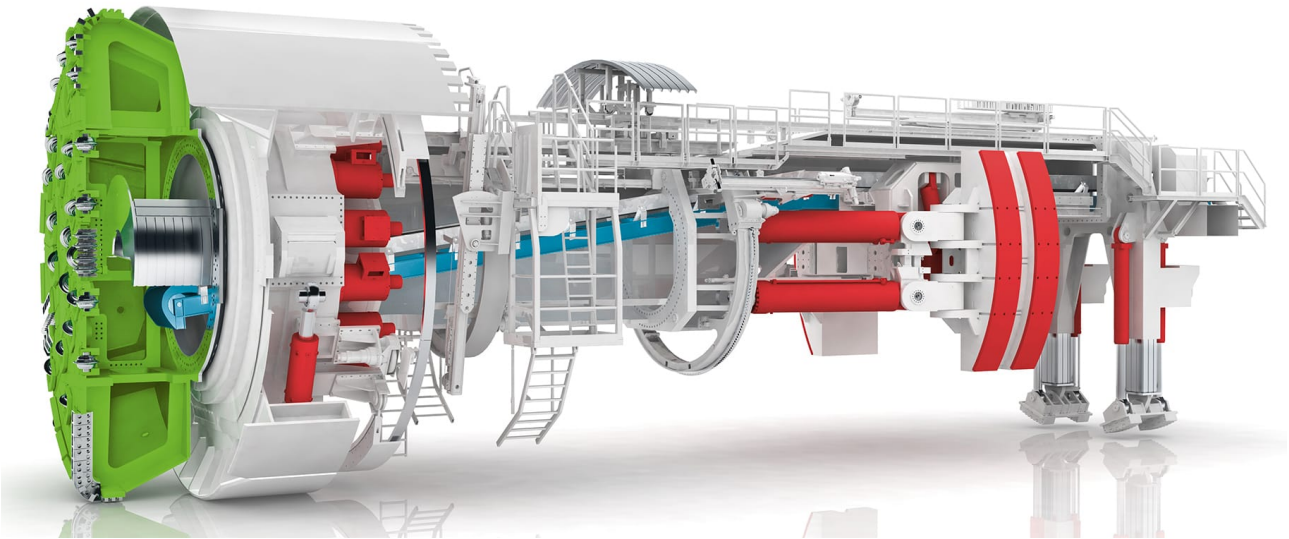

Figure 3: Open TBM. Image courtesy of Herrenknecht

2.2 Mono-shield TBM

Some rock formations may be heavily fractured, leading to increased risk of collapse and machine entrapment. The logical solution to this is to install a shield directly behind the cutterhead, which is usually segmented to allow for smooth curve transitions along the tunnel axis. As the rock is unstable, tunnel segmental linings are installed behind the shield through the use of a conveyor belt and a segment erector.

Unlike in open TBMs which push against grippers in the advancement, mono shields use smaller jacks (beneath the shield) which push against the newly installed segment lining around the bored tunnel. Once the machine has been extended to its maximum, the jacks are retracted and a tunnel lining segment is installed, the jacks are then set against the lining and the excavation may continue.

The segments are usually carried up to the erector in batches by the conveyor belt. After installation, grouting is injected through special holes in the lining.

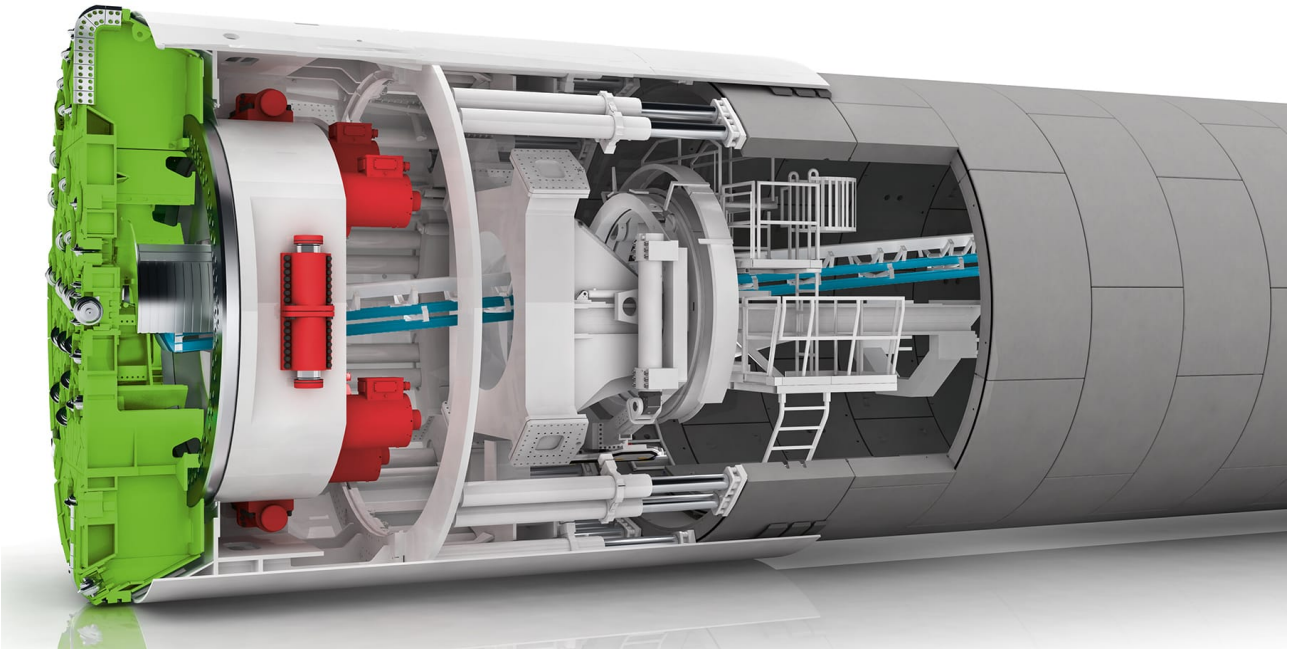

Figure 4: Single shield TBM. Image courtesy of Herrenknecht

2.3 Double-shield TBM

The double shield TBM is a serious advancement compared to the mono shield. It is also very versatile as it is capable of handling a diverse range of rock conditions. The working principal combines aspects from the mono shield, and open TBMs.

The cutterhead and its primary forward shield extend forward through the use of hydraulic jacks which push against a set of grippers. As this is happening, the secondary telescopic shield becomes extended and covers the gap as the machine moves forward. Since the grippers are stationary, the segmental linings can be installed behind them at the tailskin almost immediately, even when the cutterhead is still moving forward. Once the lining is installed, the auxiliary jacks behind the gripper can push against the lining and the front of the machine moves forward, allowing the grippers to be repositioned. The lining installation takes place exactly like with a mono shield. The process will then repeat itself until the completion of the tunnel.

This system thereby increased productivity as the lining can be installed during excavation. Excavation is then only stopped to readjust the grippers, making the whole process much faster. Another advantage is that if the machine encounters heavily fractured rock which does not allow the grippers to exert a pressure on the rock face to anchor the machine in place, it can simply retract the primary jacks and operate as a mono shield, and pushes against the segment lining with the auxiliary jacks.

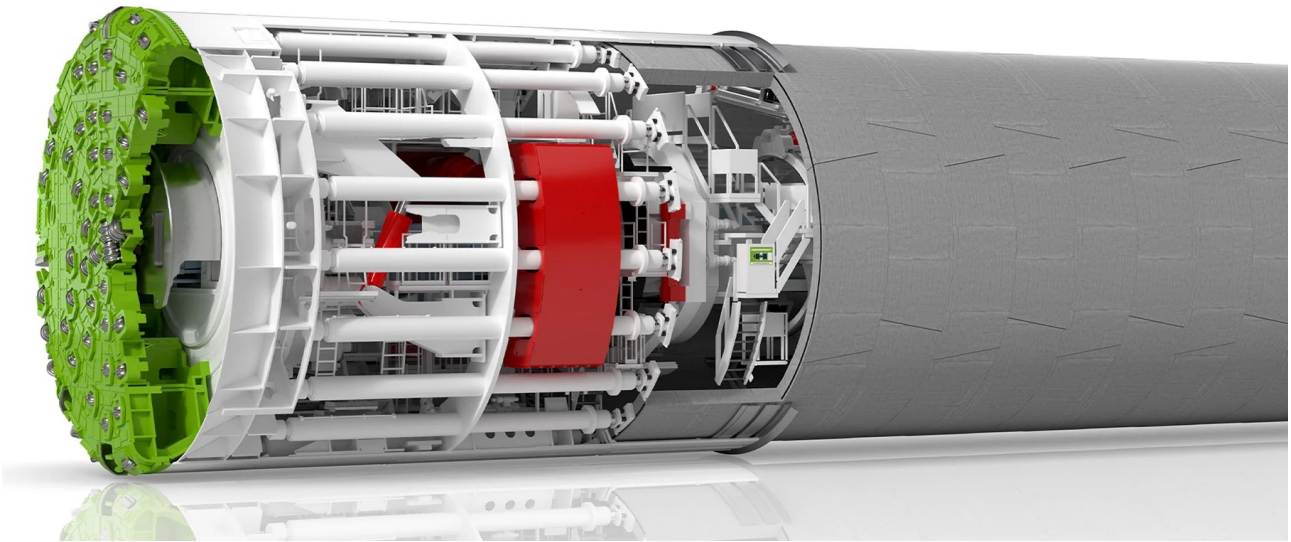

Figure 5: Double shield TBM. Image courtesy of Herrenknecht

2.4 TBM speed comparison

In the existing literature, there is not much in the way of direct comparisons for the speeds of different machine types operating in various rock conditions. Rather, there are some isolated studies offering insight into the matter. More often than not however, a lot of the studies look at and compare the wear and efficiency of the cutters, as concrete information on speed comparisons is not readily available due to the immense number of possible variables. That being said, some information has come to light. For instance in their study, “Performance Analysis of Tunnel Boring Machines for Rock Excavation”, Marilena Cardu et al. were able to identify that double shields machines can achieve a higher advancement rate than the single shield machine type.

The same authors also highlighted the fact that correlations between machine parameters and advancement rates presented many problems, namely because the literature observed only covered tunnel length and total duration. However, they postulated that the overall speed would be different for the same sort of machines with the same diameters, giving a wide range with the maximum being 1000 m/month and the low end being less than 200 m/month. They then suggested that even though this information might be adequate for initial assessments, more data points will be needed if future studies are to be conducted.

A study out of South Korea detailed a series of tunnel works utilising various TBM types, and the authors were able to present information on the advancement rate. They showed the data for specific parameters of 5 tunnel projects which may be helpful on a larger scale when compared with other data when it is available. In TBM Performance and Development State in Korea, S. W. Lee et al. recorded the following data in figure 6:

Table 1: Records of TBM advance rate

	Jukryeung Tunnel	Bookak Tunnel	Busan subway (section 203)	Kwangju city rail line I	Seoul subway (section 909)
TBM	Open TBM	Open TBM	Slurry Shield TBM	EPB Shield TBM	Slurry Shield TBM
TBM outside diameter (m)	4.5	5.0	7.3	7.4	7.8
Advance rate (m/day)	48~55.2	48.0	14.4~19.0	10.1~25.9	28.1~32.9
Average daily advance rate (m/day)	16.6~17.2	10.0	1.4~5.2	0.6~9.4	5.6~6.7
Operation rate (%)	31.2~34.6	20.8	9.7~27.4	5.9~36.3	19.9~20.4

Figure 6: Table of advancement rates in South Korean tunnels. Adapted from S. W. Lee et al. (2011), table 1

The Chinese study, A TBM advance rate prediction method considering the effects of operating factors, discussed the various factors affecting the advancement rate. From the data that was analysed, the authors were able to create some mathematical models capable of predicting the advancement rate in limestone. This was done by considering geological and machine parameters. They also stated that the deviation between the

prediction model and the actual advancement speed was within a 25% margin of error. Figure 7 tabulates their results.

Table 9
TBM advance rate prediction in limestone strata.

Chainage section	J_v (Number/m^3)	R_c (MPa)	Classification of rock mass	Predicted P/mm	Predicted N(r/min)	Predicted AR(m/h)	Actual AR(m/h)	Deviation of AR (%)
70744 ~ 70708	10.4	55	III	8.87	5.94	0.97	0.78	23.72
70025 ~ 69990	19.0	56	IV	12.58	5.20	0.67	0.64	10.54
69158 ~ 69080	10.4	44	III	10.41	5.94	1.04	1.32	−21.38
68858 ~ 68766	4.8	68	II	7.29	6.68	1.09	1.31	−17.15
68730 ~ 68710	21.4	64	IV	14.87	5.20	0.68	0.66	3.38
67542 ~ 67500	21.8	75	IV	10.95	5.20	0.66	0.69	−4.16
66300 ~ 66100	19.7	55	V	14.37	5.20	0.66	0.59	13.23
63122 ~ 63030	5.4	65	II	7.98	6.68	1.15	1.11	3.56
59801 ~ 59707	10.2	48	III	9.58	5.94	1.00	0.92	9.62

Figure 7: Table of advancement rates in Chinese tunnels. Adapted from Liu-jie Jing et al. (2021), table 9

In the same study, they also showed the down time and operating percentage for TBMs operating in different rock mass classes, seen hereunder in Figure 8:

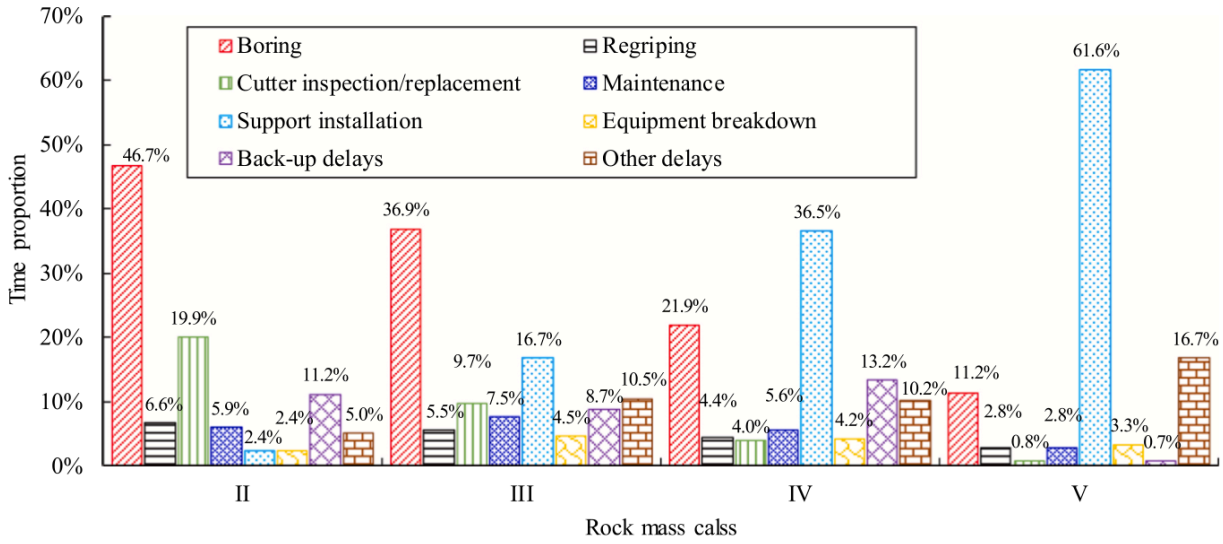

Fig. 11. Time statistics of the TBM construction process for different rock masses.

Figure 8: TBM operational times. Adapted from Liu-jie Jing et al.(2021), figure 11

The authors also concluded that their study was limited due to the varying geological nature of tunnel projects as well as a lack of diverse datasets.

An Indian case study by Prasnna Jain et al., Performance Characteristics of Tunnel Boring Machines and Correlation with Empirical Prediction Model - Case Study From Mumbai, India, provided prediction results using the Graham method for various rock types, reported below in Figure 9:

Table 3
TBM Penetration Rates for Different Rock Types

		UCS kN/m² Thrust/Cutter (kN/cutter)	TBM performance at maximum design thrust/ cutter and Max. RPM				TBM performance at different operational thrust/cutter and RPM as per actual ground conditions				Based on Graham (1976) model	Actual penetration rate achieved
			Penetration per revolution (mm/rev)	RPM	Penetration rate (m/hr)	Thrust/Cutter (kN/cutter)	Penetration per revolution (mm/rev)	RPM	Penetration rate (m/hr)	Ave. penetration rate (m/hr)	Ave. penetration rate (m/hr)	
Fine compact basalt	Min	33350	123	14.59	14	12.25	44.90	5.3	10	3.18	2.06	2.15
	Max	115900	123	4.20	14	3.53	78.02	2.65	8	1.27		
	Average	78200	123	6.22	14	5.23	63.43	3.2	9	1.73		
Porphyritic basalt	Min	115800	123	4.20	14	3.53	67.35	2.29	9	1.24	1.16	1.49
	Max	143330	123	3.39	14	2.85	84.19	2.31	7	1.10		
	Average	130600	123	3.73	14	3.13	78.02	2.35	8	1.13		
Amygdaloidal basalt	Min	54100	123	8.99	14	7.55	28.06	5.44	11	2.02	2.08	2.07
	Max	65700	123	7.41	14	6.22	61.74	4.41	10	2.22		
	Average	59800	123	8.41	14	6.83	42.10	5.13	10	2.0		
Tuff breccia	Min	26430	123	18.41	14	15.46	36.48	5.44	12	3.92	3.32	3.11
	Max	50200	123	9.69	14	8.14	56.13	4.41	10	2.64		
	Average	34460	123	14.12	14	11.86	44.90	5.13	11	3.39		
Tuff	Min	15680	123	31.03	14	26.06	19.65	4.94	4	1.18	1.88	1.80
	Max	24280	123	20.04	14	16.83	31.43	5.10	6	2.84		
	Average	18400	123	26.44	14	22.21	25.26	5.41	5	1.62		
Shale	Min	28300	123	17.09	14	14.44	36.48	5.44	12	1.64	2.30	2.60
	Max	34350	123	14.16	14	11.90	56.13	4.41	12	3.01		
	Average	31320	123	15.53	14	13.05	44.90	5.13	11	2.24		

Figure 9: Penetration rates in different rock types. Adapted from Prasnna Jain et al. (2015), table 3

This available data was then gathered and attempts at finding patters between them were made. Of course, this short analysis is severely limited due to the difference in machine parameters, geological conditions, tunnel diameter, and any other potential unforeseen variables. Some assumptions also had to be made due to the inconsistent data, such as the rock class. Some of the studies did not identify the class, but instead provided the type of rock or other conditions. This data was compared with the existing literature to try and match the appropriate rock class and in doing so, reduce the number of unknown variables. Figure 10 represents all the data.

Case Study	Location/Section	TBM TYPE	TBM Diameter (m)	Cutter Disk sieze (")	Rock Type	Rock Class	Adv Rate (m/hr)	Avg adv rate (m/hr)	Predicted AR(m/h)	Actual AR(m/h)	Notes
CHINESE STUDY	70744~70708	OPEN	7.9	17		III			0.970	0.780	Study did not specficy type of TBM used but largely concerned itself with OPEN TBM types
	70025~69990	OPEN	7.9	17		IV			0.670	0.640	
	69158~69080	OPEN	7.9	17		III			1.040	1.320	
	68858~68766	OPEN	7.9	17		II			1.090	1.310	
	68730~68710	OPEN	7.9	17		IV			0.680	0.660	
	67542~67500	OPEN	7.9	17		IV			0.660	0.690	
	66300~66100	OPEN	7.9	17		V			0.660	0.590	
	63122~63030	OPEN	7.9	17		II			1.150	1.110	
	59801~59707	OPEN	7.9	17		III			1.000	0.920	
KOREAN STUDY	Jukryeung Tunnel	OPEN	4.5	NO DATA		III	2.150	0.704		0.704	1) No data provided by authors on exact geology - consulted other sources. No information was found for any of the sites except Busan which features principally igneousand sedimentary rocks. 2) Actual AR uses avg adv rate
	Bookak Tunnel	OPEN	5	NO DATA		III	2.000	0.417		0.417	
	Busan Subway	SLURRY	7.3	NO DATA		III	0.696	0.138		0.138	
	Kwangju City Rail	EPB	7.4	NO DATA		III	0.750	0.208		0.208	
	Seoul Subway	SLURRY	7.8	NO DATA		III	0.256	0.256		0.256	
INDIAN STUDY		OPEN	3.6	17	SHALE	IV			2.300	2.600	
		OPEN	3.6	17	TUFF	III			1.880	1.800	
		OPEN	3.6	17	TUFF BRECCIA	III			3.320	3.110	
		OPEN	3.6	17	AMYGDALOIDAL BASALT	III			2.080	2.070	
		OPEN	3.6	17	PORPHYRITIC ROCK	III			1.160	1.490	
		OPEN	3.6	17	FINE COMPACT BASALT	II			2.060	2.150	

Figure 10: Advancement rate case study comparison

3. Rock cutting and working principals

Rock cutting revolves around various principles concerning the cutter discs and the effect of the rock on them. Having an understanding of this is crucial as this will ensure a better assessment of effects of rock morphology on the machinery and how to best deal with specific scenarios.

3.1 The cutter disks

The cutter disks are crucial components to the smooth operation of the TBM. These disks are the primary means of excavating the rock face and thus experience a very high degree of wear and tear, especially when considering the fact that various rock types will have varying geological parameters.

3.2 Cutter disk types and design parameters

The rock composition is the leading cause of the cutter disk decay, leading to less efficient excavation. For this reason, the disks have been designed to have a self sharpening profile with a tip thickness between 12mm and 30mm. When the rock is of a high strength and a low abrasive mineral content (feldspar, quartz, etc), a smaller tip thickness is optimal. Larger cutter tip thicknesses are then preferred for rocks characterised as having medium and low mechanical strength, and the abrasive mineral content is usually ignored. Figure 11, by Palmieri SpA, is a good illustration depicting the shapes and tip thicknesses of the disks.

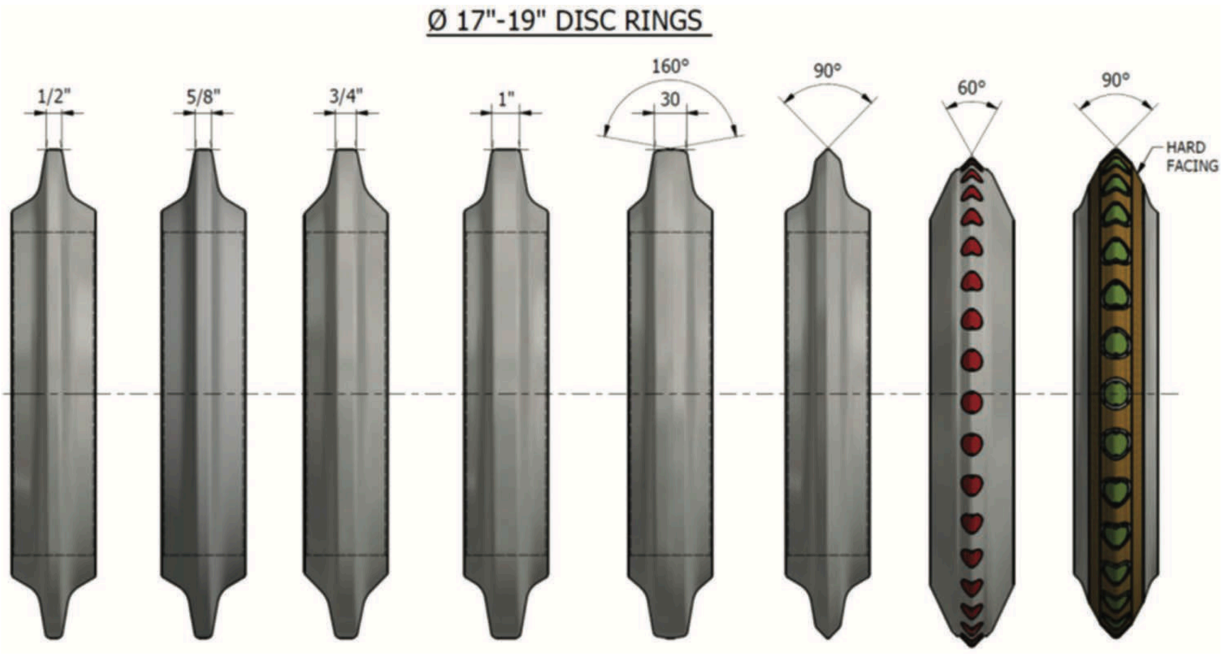

Figure 11: Cutter types. Reproduced from P. Grasso et al. (2023), figure 2.32, originally by Palmieri SpA

Over the years, various types and sizes of discs have become available, however, the industry standard diameter has now become the 17” and 19” disks. In some cases, when there is a high percentage of quartzite which is very abrasive, 20” diameter cutter disks can also be used. The selection of the diameter size is largely dependent on geological

parameters with the abrasiveness and mechanical strength being the main influencers affecting the total penetration and wear of the cutter disk. The bigger disk sizes have more usable cross sectional area, which leads to less wear as it is spread over a larger area. The penetration also increases as does the cutter life. In the presence of very strong rock, the minimum cutter disk size is set at 17”, as using larger discs in harder and more abrasive rock will permit less cutter changes in terms of excavated cubic meters. This then lowers the operating costs.

Sometimes, the machine will need to tunnel through soft rock with a high abrasive mineral content, and in these cases, the larger diameters are also used. This might seem counterintuitive especially when the machine might have been designed to have certain maximum parameters for penetration, torque, etc, which can be catered for with a smaller diameter disk. In this way, the wear on the disk can be reduced.

In terms of cutter material, the standard is to use a steel alloy, with varying amounts of manganese content which is then heat treated accordingly. Disks with a higher percentage of manganese are best suited for more heavy duty applications. Using this alloy enables the cutters to be more resistance to wear, however, there is an increased risk of the cutters breaking when used in mixed or fractured rock conditions when compared to mixed with a much lower manganese content. Obviously, treating the metal in such a way will greatly increase the cost, and thus the rule of thumb is to use the heavy duty cutters when hard and abrasive rock will be encountered.

The cutters can also come equipped with so-called tungsten carbide inserts, which improves the penetration rate of the cutter in high strength rock formations. From field data, it has been observed that the cost to use time ratio is not that favourable. That being said, they have proven themselves to be the best option for obtaining adequate penetration rates in the harshest rock conditions. The authors of “Volume 2 of Handbook on Tunnels and Underground Works” detail a cutter disk with tungsten carbide inserts in figure 12. Examples of the type of wear experienced by the disks were also published by the same authors and can also be seen in the same figure.

Figure 12: Cutter with tungsten carbide inserts, left. Cutter wear examples, right. Adapted from P. Grasso et al. (2023), figures 2.34 and 2.35

An important point to consider, is that the cutter disks are not only effected by the rock, but also by the thrust applied onto them by the machine, so much so that each disk size has its own ideal maximum net thrust that it may be allowed to experience. The 19” cutters can handle up to 320 kN of thrust, while the smaller 17” work best up to 245 kN of thrust. This is important information that must be kept in mind during the design phase of the TBM’s construction, as a balance must be found between all the forces acting on the cutters to ensure that they are sufficiently strong enough to withstand final net thrust after considering all the mechanical stresses taking place. Failure to do so will lead to inefficiencies when the cutters are actually cutting the rock and thus negatively effecting the volume of excavated material in relation to cutter wear.

It can be appreciated that the cutters are under considerable stress, which is transmitted to the smaller mechanical components that allow the disks to rotate. These can be seriously damaged if not well taken care of. For this reason, the inner workings of the cutter disks such as the bearings, must be well lubricated. In some applications, normal lubricant is not enough and specialised greases have been used to prevent damage to the delicate bearings. Figure 13 has also been provided to offer an internal view of the moving parts within the cutter disk housing, in this case the bearings are of the tapered roller type.

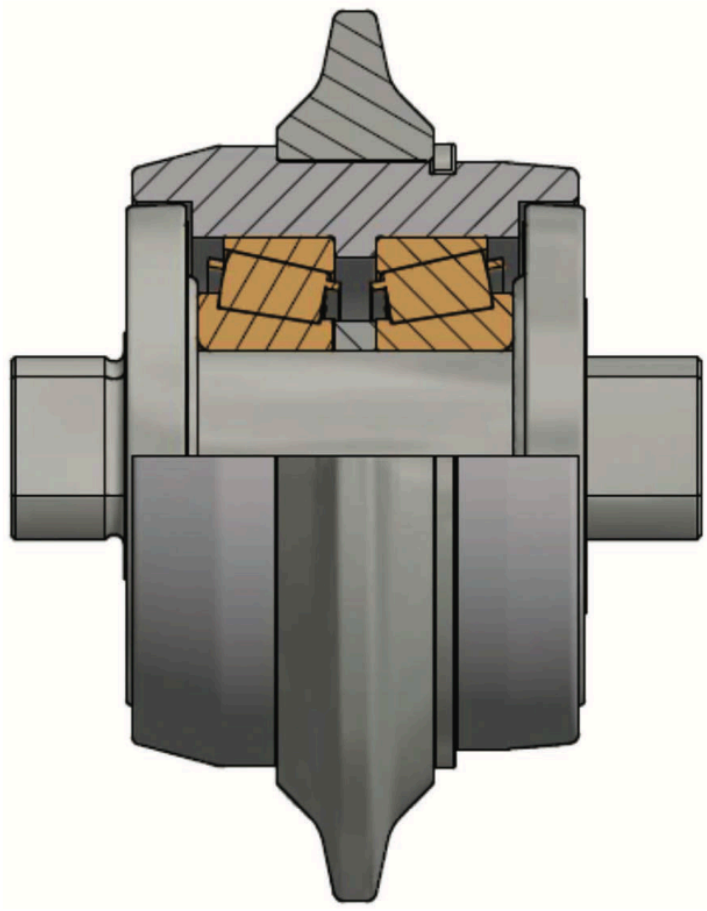

Figure 13: Cutter disc with section showing bearings. Adapted from P. Grasso et al. (2023), figure 2.36

3.3 Cutter disk working principals

Excavation is made possible when the TBM applies a forward thrust onto the rock face via the on board hydraulic cylinders and at the same time, the cutterhead (which houses the cutter disks) rotates. The forward thrust force which is normal to the rock face is characterised as F_N, while the rotational movement creates a tangential rolling force, F_R. Together, these forces help create the phenomena of rock chip formation which is when the cutters are able to penetrate and fragment the rock.

At present, there is ongoing debate as to what is the main precise means and relevant explanation for the rock fragmentation process. That being said, it is evident that rock chipping occurs due to traction forces which create a radial pulverised bulb around the cutter, whilst fragmentation takes plays under the action of shear forces.

The radial pressure bulb model was developed by the Colorado School of Mines, in which they were able to produce accurate predictions for the performance of the cutter disks on the TBM. Experimentation deduced that the forward pressure applied by the machine into the cutters is transferred to the rock face during penetration, creating the so called pressure bulb. This bulb is essentially the zone where the rock becomes pulverised with radiating tensile cracks forming outwards. When cracks intersect each other (due to other neighbouring disks at a specific spacing), chips begin to detach. It was also understood that the fragmentation occurred when the cutters created lateral fractures emanating from the chips around the cutter tip. Figure 14 by Huipeng Zhang et al. (2024) perfectly represents both the crushed zone alongside the pressure bulb, and chip formation.

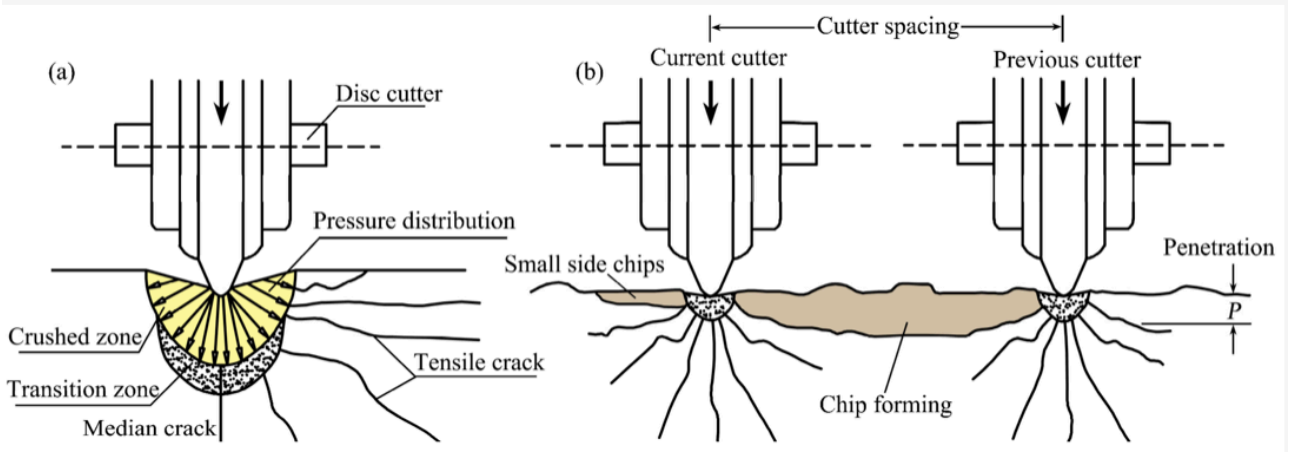

Figure 14: Crushed zone and pressure bulb during disc penetration. Adapted from H. Zhang et al. (2024), figure 13

It is also believed that there is another means by which fragmentation occurs. When the rock is very hard, multiple rotations of the cutterhead are needed to achieve breakage of the rock. As the cutterhead rotates, multiple discs pass over the same location, leading to a repeated force applied to that area for a varying amount of time which will ultimately lead to the fragmentation of the rock. Some other observations regarding the marks and debris left behind by the cutters on the rock face were also made, as highlighted in page 83 of “Volume 2 of Handbook on Tunnels and Underground Works”. In high mechanical strength rocks, there is a fine crushed rock powder in the groove marks of the cutters. This contrasts weaker rocks where next to no fine dust is produced - indicating that perhaps the rock is so weak that the force applied by the cutter is enough to penetrate and break part of the rock before it is able to be crushed.

3.4 Cutter disk specific energy of excavation

The specific energy of excavation is defined in “Volume 2 of Handbook on Tunnels and Underground Works” as “the energy required to excavate a unit volume of rock for a given depth of instantaneous penetration”, is an important factor that helps deduce the optimum cutter spacing, for which there is a minimum critical value as well as a maximum value. When the spacing value deviates away from these, the efficiency of excavation will be reduced. The correct design of the cutter spacing will allow for efficient penetration, even if the cutters experience some wear. It should also be kept in mind that this investigation is based on the rock with the most hardness along the alignment of the tunnel.

The specific work associated with the cutters excavating the rock can provide a very good numerical basis capable of linking penetrative and rolling forces with cutter’s size and angle of attack, as well as with the volume of excavated material per unit length of disk travel (also known as the yield). Recent studies have shown that an increased cutter diameter will require a larger thrust force to maintain penetration while the rolling force and specific energy remains constant. It was also found that the thrust and rolling forces must increase if penetration is increased, and specific energy will thus decrease. Lastly, when the angle between the disk and rock face increases, the rolling force appears to decrease while the specific energy and penetrative force increase.

The specific energy is also a telling sign of how fracture will take place in the rock. Page 88 of “Volume 2 of Handbook on Tunnels and Underground Works” stipulates that based on fracture mechanic principals, the fracture lines will adopt the lowest specific energy direction. This then means that any fracture angle is capable of producing rock fragments. Evidence of this usually emerges when over-excavations are present, in which the rock fragments are small triangular pieces when compared to the normal fragments.

4. TBM performance prediction models

Various prediction models exist to evaluate crucial parameters that need to be known for the design of both the TBM and the tunnel. Cutter wear, rate of penetration, net volume of rock excavated, and cutter life index are just some of the measurable parameters, and are used at various stages of the design process.

These models can be considered to be either Analytical models where theoretical studies are carried out, or Empirical models, which are based on a vast array of datasets from previous projects.

4.1 Analytical Models

The basis of analytical models revolves around the use of mechanical tools to initiate rock fragmentation. Various laboratory tests have been carried out, namely the punch penetration test and linear cutting test, which focus on the forces that act on the cutter. It is then from these test results that it is possible to define the power requirement, torque, and thrust of the TBM.

These models are not without drawbacks however, as they utilise characteristics of intact rock alongside cutter parameters, without accounting for the characteristics of the rock mass. this means that it is usually the σc and σt as well as cutter diameter, tip type, spacing, etc being analysed against joint orientation and frequency.

The 1970s was when the earliest tests took place. V-cutters for cutting force models were used (they are no longer used today) as well as laboratory test. In recent times, main reference is made by Ramezanzadeh (2006), Ramezanzadeh et al. (2003), and Oggeri & Oreste (2012).

4.11 Colorado School of Mines Model

General overview

The Colorado School of Mines developed a rigorous model under the guidance of Rostami & Ozdemir, in 1993. The model not only relies on linear cutting test results, but also on mathematical assumptions for the fragmentation of rock.

The CSM model makes use of the previously mentioned pressure bulb where the rock is crushed beneath the cutter tip, and is assumed to be circular with a decreasing stress at points further away from the tip contact zone. The authors imposed that the pressure in the bulb is uniform as they did not know the actual distribution, and the fracture length was designated as being a function of the pressure in the crushed area. This is then related to the normal thrust force F_N that acts on the cutter. It is also more efficient to ensure a correct cutter spacing to not have over break or ridge formation when there is excessive load or a lack in pressure respectively.

It can also be said that there is a pressure distribution on the cutter's surface where the cutter and rock meet, and since constant pressure distribution implies balanced forces, it is considered to be two dimensional. By knowing the total thrust of each cutter, it is possible to determine the required force per cutter to achieve penetration. Working off this value, the torque, rotational speed, total thrust and required power can be defined.

In subsequent years, the model was adapted by Rostami in 2008, while in 2010, Frenzel was able to incorporate predictions for cutter wear by considering disk cutter life (CL), the Cerchar Abrasive Index (CAI) and the disk diameter. Together, these parameters help find the rock volume excavated per cutter. Then in 2003, Ramezanzadeh et al included joint angles and spacing.

The method also relies on the following bands of parameters for tunnels in North America:

- $70 < \sigma_c < 200$ MPa
- $4 < \sigma_t < 18$ MPa
- $15 < \Phi_{disc} < 19$ inches
- $2.5 < p < 30$mm

These values can be deemed as being the bounds of operation for this model. It should be noted that when comparing the results of the different methods, it must be ensured that the input parameters are the same to ensure homogeneous conditions for all prediction model scenarios. At the same time, they must also fall between the previously stated boundary conditions. In doing so, more precise results can be obtained for a specific set of soil and machine conditions.

The method

Since two dimensions are considered, the interaction angle (in radians) which is essentially the angle between the rock and disk can be defined as follows:

$$\Phi = \cos^{-1}\left(\frac{R-p}{R}\right)$$

In which;

- R: cutter radius, mm
- p: penetration per revolution (also denoted as PR in some cases), mm/rev. For the comparison, this value should be set equal to the obtained penetration such as i_0 from the NTNU model.

The pressure magnitude in MPa, defined as:

$$P = P'\left(1 - \frac{\Theta}{\Phi}\right)^{\Psi}$$

In which;

- Θ: angle between normal and face, °
- P': base pressure (also denoted as P_r in some cases), MPa
- Ψ: independent value coefficient, 0 for uniform pressure and 1 for linear pressure distribution

Figure 15 by Rostami and Ozdemir (1993), depicts the forces and pressure distribution on the disc.

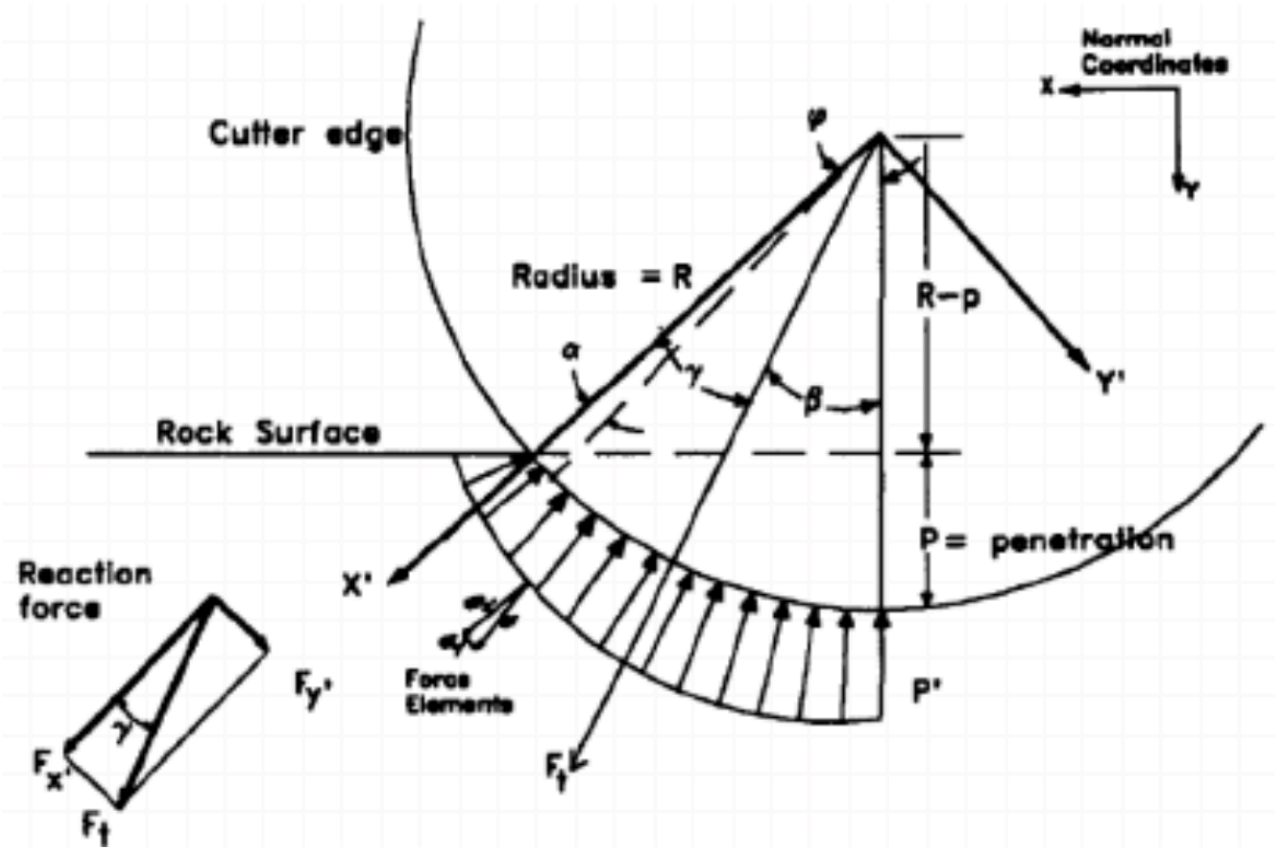

Figure 15: Rock/tip and surface pressure distribution and model parameters. Adapted from Rostami & Ozdemir, (1993)

The base pressure uses empirical data and is defined as follows:

$$P' = 2.12\sqrt[3]{\frac{S \cdot \sigma_c^2 \cdot \sigma_t}{\Phi\sqrt{R \cdot T}}}$$

Where;

- S: cutter spacing, mm
- σ_c: uniaxial compressive strength, MPa
- σ_t: intact rock tensile strength, MPa
- T: cutter disk tip width, mm

The value of 2.12 is a standard one which is used most of the time, however, there could be specific values depending on the scenario in which case it may be edited. For the purposes of this work, it was kept constant as 2.12.

The force acting on the cutters during excavation (in Newtons) is defined hereunder:

$$F_{tot,cutter} = \frac{P' \cdot R \cdot T \cdot \Phi}{\Psi + 1}$$

The authors of the CSM method also established that this force can be expressed in a different way, for when the pressure is uniform. This means that the Ψ becomes zero and the base pressure P' is said to be equal to the pressure magnitude P:

$$F_{tot,cutter} = 2.12 \cdot R \cdot T \cdot \Phi \cdot \sqrt[3]{\frac{S \cdot \sigma_c^2 \cdot \sigma_t}{\Phi \sqrt{R \cdot T}}}$$

As there are various equations for force acting on the cutters, an operation was included to automatically choose the correct equation and therefor value, depending on whether the pressure is uniform or linear.

This total cutter force is a resultant of the following components, the normal force F_N and the rolling force F_R:

$$F_N = F_{tot,cutter} \cdot \cos\left(\frac{\Phi}{2}\right)$$

$$F_R = F_{tot,cutter} \cdot \sin\left(\frac{\Phi}{2}\right)$$

The normal force must also be within a certain bounds, depending on the disk being used. The conditions are implemented in the program to show if the force is within range or not. If the boundaries are not respected, a new starting initial penetration value must be used, and the process can start again. The values related to each disk are reported below in Table 1:

Table 1 - Allowable Thrust				
Disk diameter		Disk support weight	Max allowable thrust	Disk spacing
"	mm	kN	N	mm
14	355.6	10	160000	60-70
15.5	393.7	12	180000	60-70
17	431.8	15	250000	70-80
19	482.6	22	30000	70-80

Table 1: Allowable thrust by cutter disc diameter - (Courtesy of Academia reference, Prof. Peila, 2023)

Together, the ratio of the two provides the rolling coefficient and is expressed as:

$$RC = \frac{F_R}{F_N} = \tan\left(\frac{\Phi}{2}\right)$$

In the program, values were obtained using both the expressions for RC, to ensure correctness.

It is then necessary to include the TBM's parameters. The required theoretical total thrust is given in kN and is the product of normal force and the number of cutters:

$$F_{tot,th} = n_{cutters} \cdot F_N$$

From this, it is then possible to calculate the theoretical torque in kNm, with the TBM diameter Φ_{TBM} in meters:

$$M_{cutterhead,th} = 0.3 \cdot F_R \cdot \Phi_{TBM} \cdot n_{cutters}$$

Rotational speed is also found in rpm and incorporates the linear velocity limit of the cutters which is known beforehand. In the cases where a 15 inch diameter disk is used, this value would be 150 m/min. This value is an input parameter which is specified by the manufacturer of the TBM.

$$v_{rot} = \frac{v_{lim,cutter}}{\pi \cdot \Phi_{TBM}}$$

The two previous equations can then be used to find the theoretical power requirement in W:

$$P_{cutterhead,th} = \frac{\pi \cdot M_{cutterhead,th} \cdot v_{rot}}{30}$$

This value can then be divided by an efficiency factor normally denoted as η, and thus it is possible to find the so called installed power and thrust by dividing the theoretical power by the efficiency factor. In most cases, η is given as 90%.

The penetration rate is then found:

$$ROP = PR \cdot v_{rot} \cdot \frac{60}{1000}$$

"PR" was taken as being "p" from the first equation.

There are however certain limits for the torque, thrust and penetration expressed as functions of σ_c, which must be satisfied, as proposed by Frenzel et al. (2012) in Figure 16:

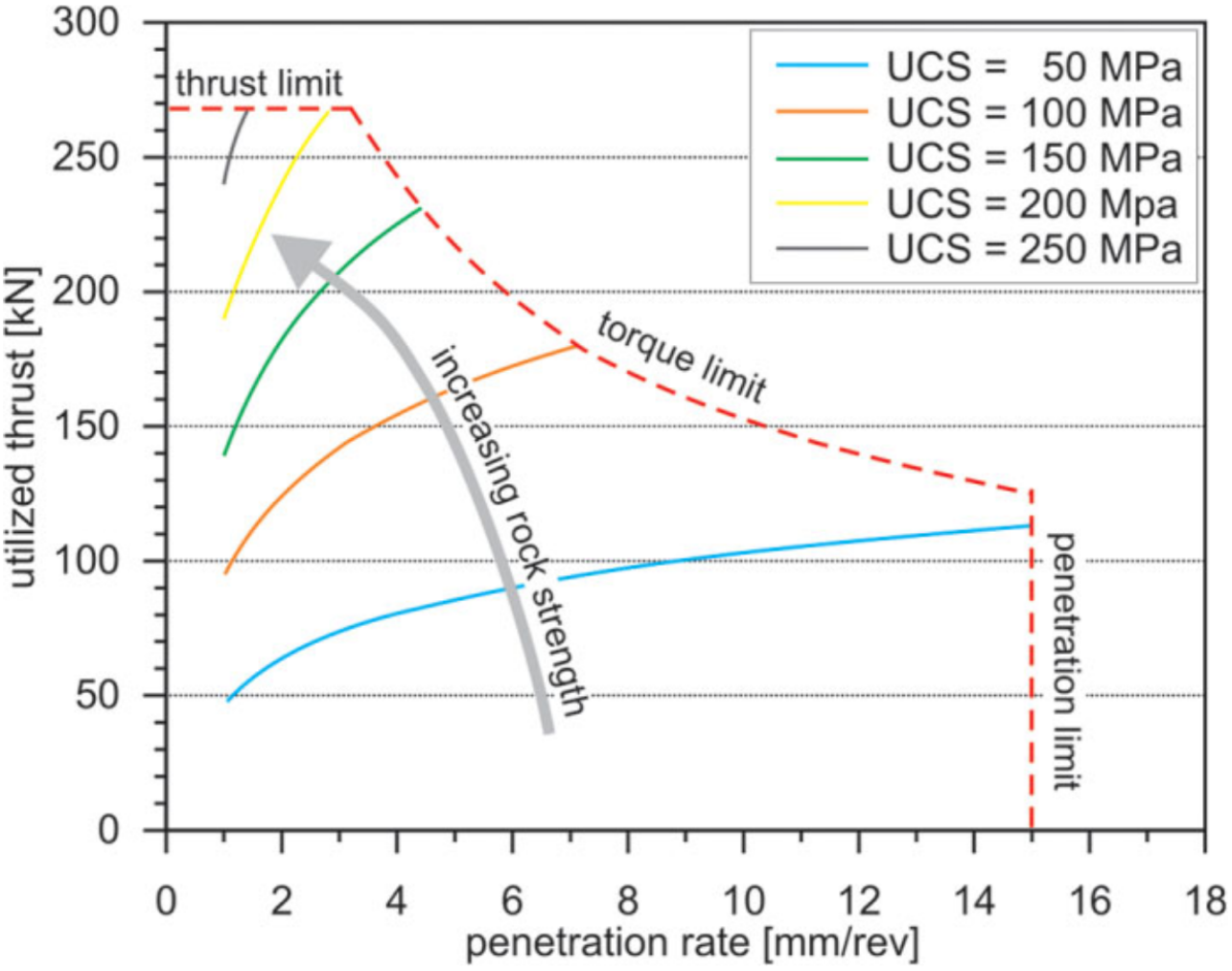

Figure 16: TBM with 17" cutter disc operating limits for different rock strengths. Adapted from Frenzel et al. (2012)

At this point, it is possible to include the work of Frenzel and Rostami, to predict the cutter's wear in terms of its drive length until wear. The Cerchar Abrasive Index (CAI) is used alongside disk diameter in inches. This value is expressed in 10^6 ft and can be seen below. The equation was also modified to provide a value in more standard terms, in this case, kilometres.

$$\Delta L_i = \frac{6.75 \cdot \Phi_{disc}}{17 \cdot CAI}$$

Frenzel also proposed the following to determine the net excavated volume per cutter until the cutter is consumed. The first step is to determine the cutter life in km, by using the disk diameter in mm from the following equation:

$$CL = \frac{2057 \cdot \Phi_{disc}}{432 \cdot CAI}$$

This value is also analogous with the previous one for drive length to wear. Having both side by side helps corroborate data.

Then, the average length the cutter experiences from every rotation is determined (in meters) by:

$$L_{av,disc} = 0.6 \cdot \pi \cdot \Phi_{TBM}$$

With the number of average rotations the cutter experiences in its life before wear being given by:

$$U_c = \frac{\overline{k} \cdot CL}{L_{av,disc}}$$

k̄ in this case is a reduction factor to account for the shape of the cutterhead, which Frenzel suggested to be 67%.

Frenzel was also able to determine the length of tunnel covered in meters until the cutter is completely worn:

$$\Delta L_c = \frac{U_c \cdot p}{n_{cutters}}$$

Finally, the net volume of excavated rock per cutter is found in m^3/cutter through:

$$\Delta V_c = \Delta L_c \cdot \left(\frac{\pi \cdot \Phi_{TBM}^2}{4} \right)$$

Some amendments were also made by other professionals to combat the fact that the CSM model does not include joint orientation and spacing. Ramezanzadeh proposed using the joint spacing J_s in [cm], and orientation α in [°] in the following equation which utilises the initially obtained ROP:

$$ROP = \frac{\left(ROP_{CSM}\right)^{0.156}}{\exp\left(0.00161 \cdot J_s + 0.00307 \cdot \left|\alpha - 45\right| - 0.596\right)}$$

This value differs from the previous ROP and is also shown in the output parameters portion of the program and can be compared with the previous one. Both values of ROP were then used to calculate net and gross excavation times for a more rigorous comparison. The procedure is the same as the final step as explained in the NTNU model.

4.12 Gehring Model

This model is semi analytical and considers the uniaxial compressive strength of intact rock. Correction factors for fracture energy, stress, joint spacing, cutter disk diameter and cutterhead diameter are also implemented.

The method

The penetration per revolution, p_{200}, is given by:

$$p_{200} = a\sigma_c^{-b}$$

Where:

- a: coefficient from table 2
- b: coefficient from table 2
- σ_c: uniaxial compressive strength, MPa

Table 2.7 Parameters for Gehring's equation from different sources

Source	*Coefficient a*	*Exponent b*
Farmer	29	0.98
Graham	78	0.99
Hughes	2,295	1.19
NTNU	3,350	1.29
Sanyo	46	1.00
Gehring (Average)	**799**	**0.99**

Source: Modified from Türtscher and Schneider (2012).

Table 2: Gehring's parameters. Adapted from P. Grasso et al. (2023), table 2.7, originally by Türtscher and Schneider (2012)

p_{200} can also be given by the following equation or figure 17:

$$p_{200} = 107 \cdot W_f^{-0.81}$$

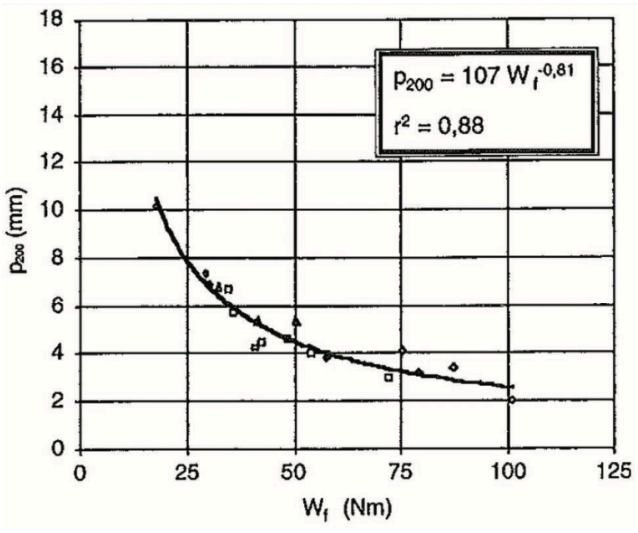

Figure 17: Base penetration. Adapted from Gehring, (1995)

A general equation was provided by Gehring as:

$$p = PR = \frac{4 \cdot F_N k_1 k_2 k_3 k_4 k_5}{\sigma_c}$$

In which:

- F_N: cutter contact pressure, kN
- k_1: correction factor for fracture energy, either via the equation or figure 18
- k_2: correction factor for spacing discontinuities and orientation, and uses figures 19 and 20. Final results are tabulated in table 3
- k_3: correction factor for stress state, no equations were specified by Gehring
- k_4: correction factor for cutter diameter, via an equation put forward by Gehring (see below)
- k_5: correction factor for cutter spacing, either obtained figure 21, in which equations were obtained via the best graphical fit for the analysis, in figure 22

Equation for k_1:

$$k_1 = 0.475 \cdot w_f^{-0.56}$$

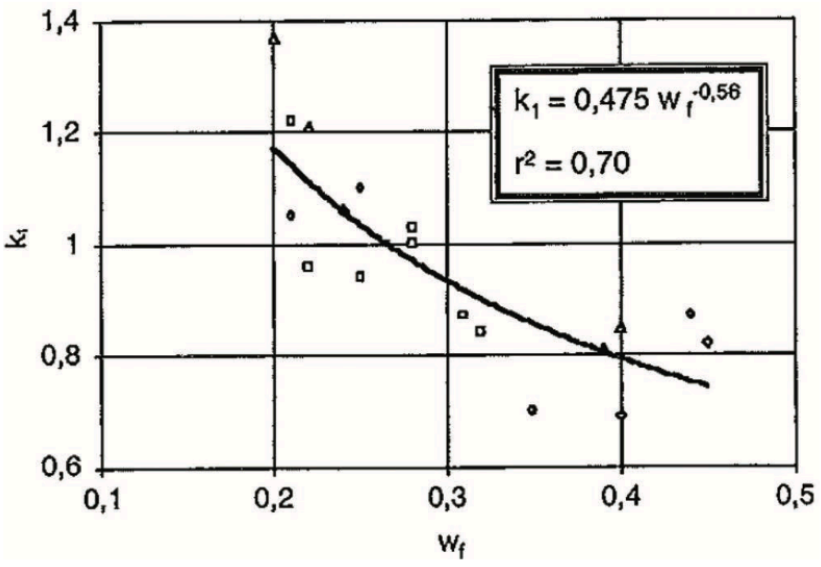

Figure 18: Correction factor k_1. Adapted from Gehring, (1995)

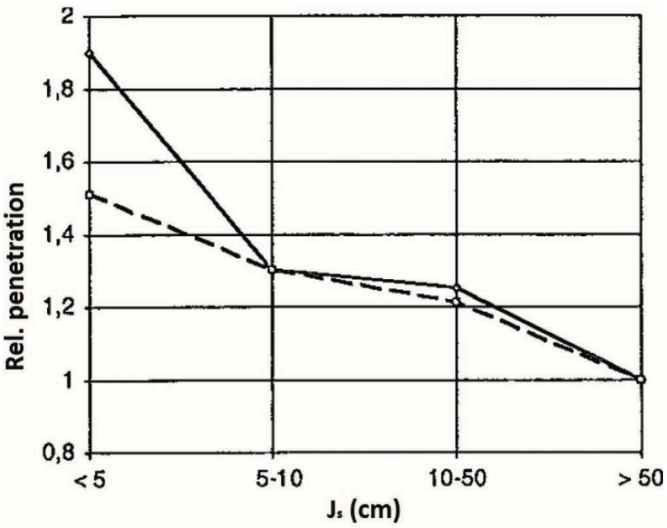

Figure 19: Joint spacing effect. Adapted from Gehring, (1995)

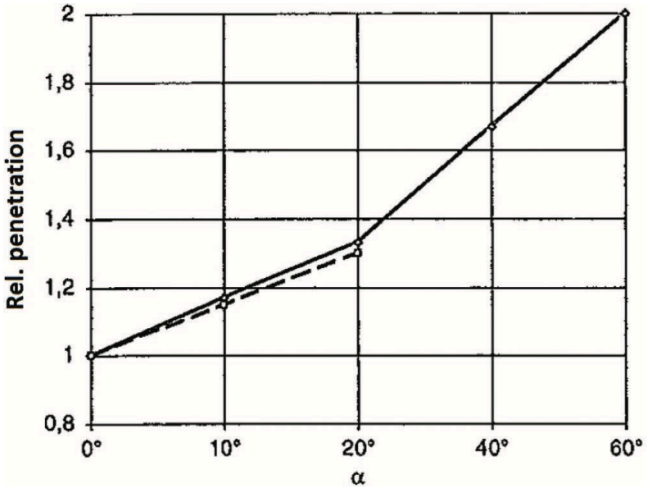

Figure 20: Joint angle effect with tunnel axis. Adapted from Gehring, (1995)

Table 2.8 Correction factor k_2 as a function of joint angle with the tunnel axis α and joint spacing J_s, Gehring

Joint spacing	*Correction factor k_2 as a function of α*			
J_s *(cm)*	*A*			
	0 (°)	*30 (°)*	*60 (°)*	*90 (°)*
>50	1.0	1.0	1.0	1.0
10 ÷ 50	1.2	1.3	1.6	1.3
5 ÷ 10	1.4	1.8	2.3	1.6
<5	1.7	2.3	3.0	2.0

Table 3: Correction factor k_2. Adapted from P. Grasso et al. (2023), table 2.8, originally by Gehring, (1995)

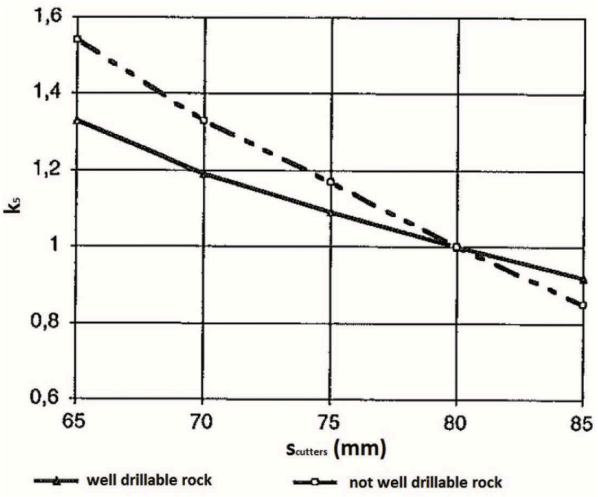

Figure 21: Correction factor k_5. Adapted from Gehring, (1995)

MY GRAPH K5

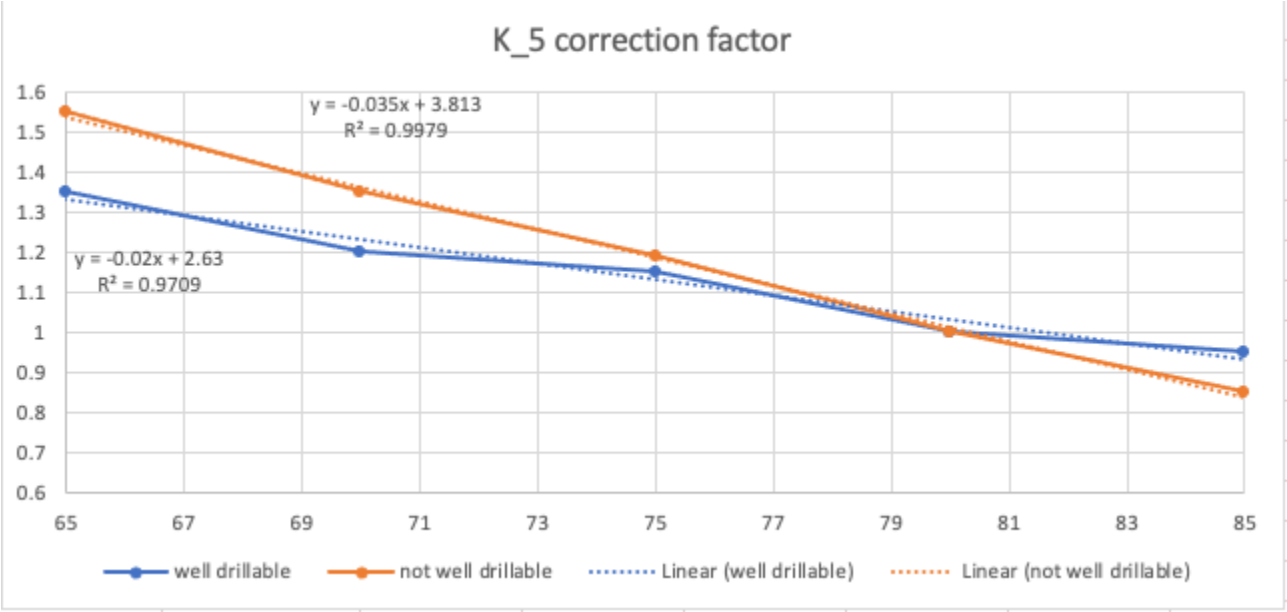

Figure 22: Re-graphing to find k_5 equations

The specific fracture energy is as follows and is in m e^6:

$$w_f = \frac{W_f}{\sigma_c}$$

In which:

- W_f: fracture energy, Nm

k_4 is given by:

$$k_4 = \frac{432}{\phi_{disc}}$$

In which:

- Φ_{disc}: disc diameter, mm

The single cutter specific loss, expressed in mg/m is expressed as follows:

$$v_s = \frac{\Delta G_i \bar{p}}{L_{disc} \,.\, \pi \,.\, \Delta L_i}$$

Or also as:

$$v_s = 0.74.CAI^{1.93}$$

In which:

- ΔG_i: cutter weight loss, g. A standard value of 3500g for a 17” cutter
- $\bar{p}$: average penetration rate, mm/rev
- L_{disc}:
- ΔL_i: meters driven until consumption, m
- CAI: Cerchar abrasive index

The driven length of consumption is expressed by the following equation:

$$\Delta L_i = \frac{\Delta G_i \bar{p}}{L_i \,.\, \pi \,.\, v_s}$$

In which:

- L_i: track distance covered by cutter, m

It is then possible to find the average tunnel length excavated before the cutter needs to be changed:

$$\Delta L_c = \frac{\Delta G_{disc} \cdot \bar{p}}{L_{av,disc} \cdot \pi \cdot v_s \cdot n_{cutters}}$$

In which:

- $L_{av,\ disc}$: cutter average path, m
- $n_{cutters}$: number of cutters

Which can be found via:

$$L_{av,disc} = 0.6\pi\phi_{TBM}$$

Finally, the excavated net volume of rock per cutter in m3/cutter is defined by:

$$\Delta V_c = \frac{\Delta L_c \cdot \pi \cdot \phi_{TBM}^2}{4}$$

In which:

- Φ_{TBM}: TBM diameter, m

4.2 Empirical Models

The advantage of empirical models is that they rely on a large database of already existing data from past projects, and having such extensive data easily accessible allows for more rigorous research approaches. Various parameters go into explaining TBM performance numerically, as do the extensive number of field parameters. With access to such information, it is possible to continuously adapt existing methods to refine the procedure and obtain more precise results, as well as facilitating the creation of new and improved models.

4.21 NTNU Model

General overview

The NTNU Model was developed by Trondheim Norwegian University of Sciences and Technology and is being continuously updated by various researchers. One of the most widespread versions was developed by Amund Bruland for his doctoral thesis in 1998. Bruland made use of a very large database with information coming from all across Scandinavia, with data of about 250km worth of tunnels in igneous rock. Cutterhead diameters for these projects varied between 2.3m and 8.5m, and compressive strength of the rock ranged between 50MPa and 250MPa. This model is able to determine the net penetration rate, gross advance rate, cutter wear, and even cost of excavation.

The data from a number of laboratory tests was also used, to better characterise the rock masses in terms of drillability. The main tests covered were Matern & Hjelmer's Brittleness Value, S_{20}, and the Sievers' J-Value, SJ, by Sievers.

The S_{20} is used to measure the repeated impact effect on rock. The value is expressed as a percentage of the crushed rock (from 20 impacts at a heigh of 25cm with a 14kg weight) that is pre sieved and then passes through a fine sieve. The final value is usually the mean value from three tests. Figure 23 is a good representation of the procedure carried out. Researchers such as Dahl et al. also showed that there is a correlation between this value and the compressive strength σ_c, as well as with Point loading strength, shown in figure 24.

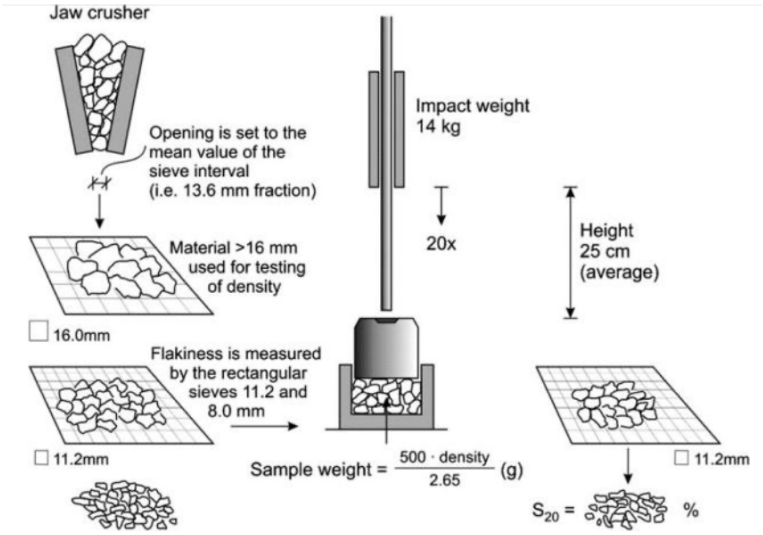

Figure 23: Brittleness value test. Adapted from Dahl et al. (2012)

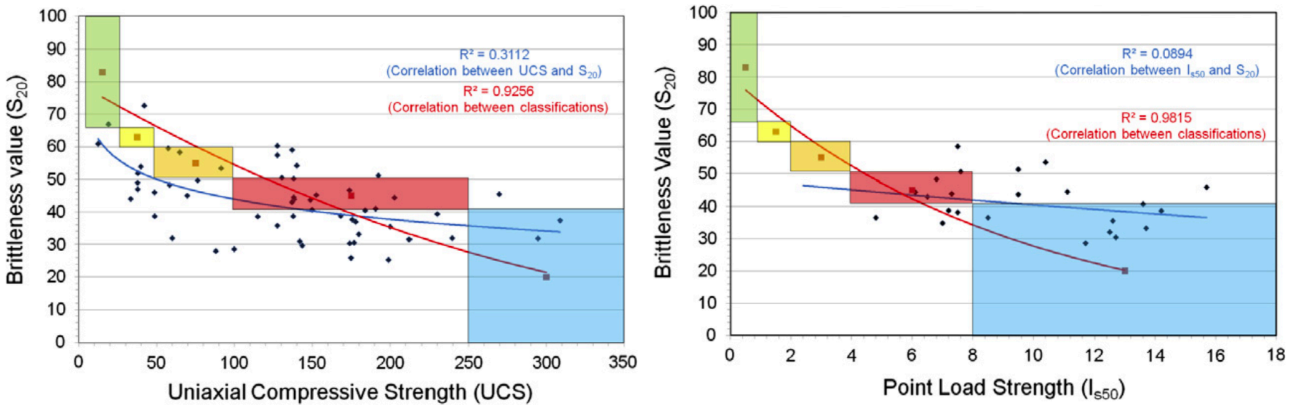

Figure 24: Correlation between S_{20} and σ_c, left and $I_{s,50}$, right. Adapted from Dahl et al. (2012)

On the other hand, the SJ value is a representation of the rock's surface hardness. The original measuring device was developed by Sievers and is a miniature 8.5mm drill bit which can be seen in figure 25. It is a mean value for drill hole depths at 1/10mm when 200 revolutions of the drill bit have been completed. The standard practice is to repeat the test for to eight times and to use a sample with a clean and pre-cut surface which is perpendicular to the rock's foliation. This implies that the SJ value is parallel to the foliation. Once more, Dahl et al. identified correlations with the parameter in question, this time in terms of the Cerchar Abrasive Index, as per figure 26.

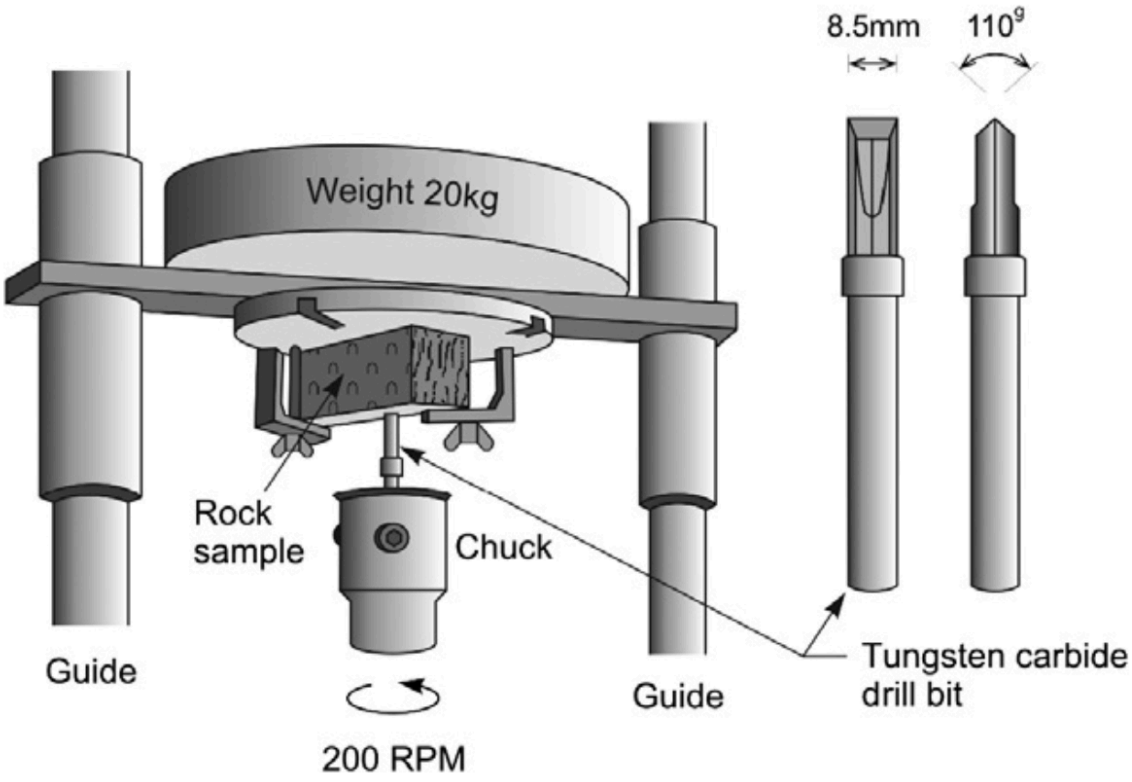

Figure 25: The Sievers miniature drill test. Adapted from Dahl et al. (2012)

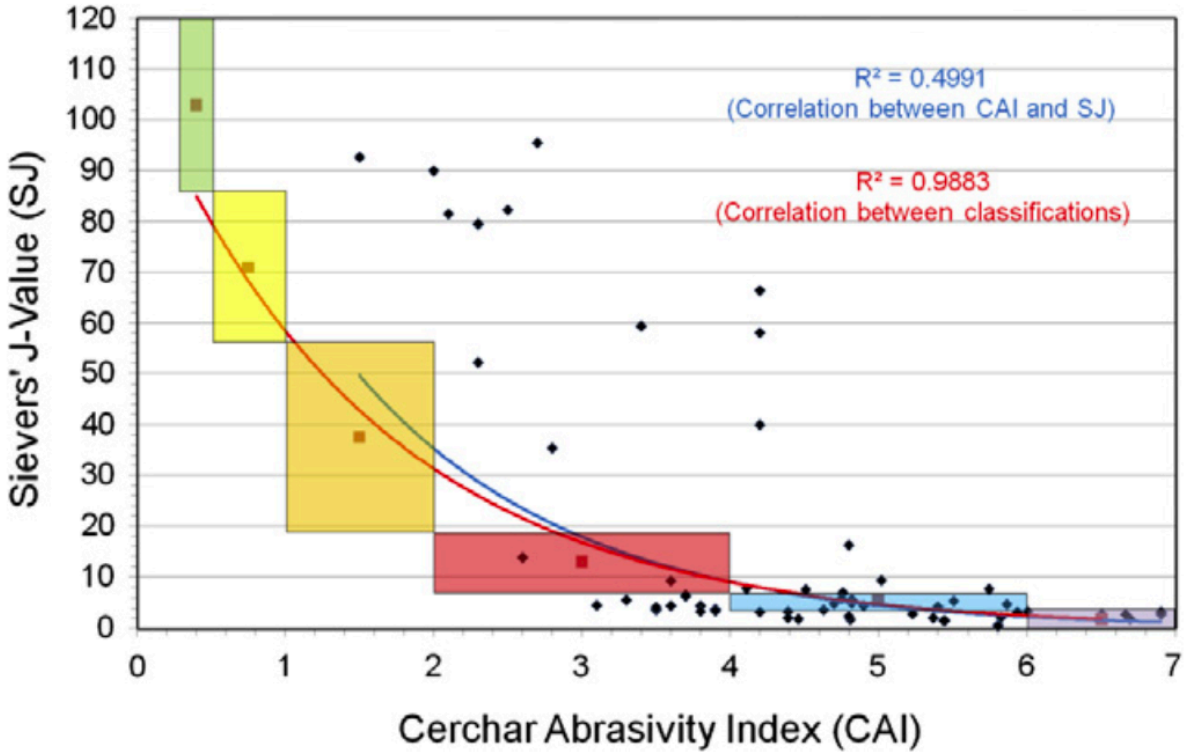

Figure 26: SJ and CAI correlation. Adapted from Dahl et al. (2012)

The Abrasion Value test, AV, and the Abrasion Value Carbon Steel test, AVS, were create by NTNU to help determine the rock abrasiveness which is an important parameter in determining cutter wear. Apparatus remains the same for both tests, with the sole difference being a tungsten carbide tip being used for the AV test and a TBM cutter steel piece used for the AVS.

During the test, the tool tip is in contact with a rotating powder covered steel disc. The powder is from rock samples and the maximum diameter is 1mm. A 10kg weight is used to press the tip onto the disk which rotates at various speeds. The test measures the weight loss of the tool tip after 5 minutes for the AV, while in the AVS it is only 1 minutes. Usually, the mean value of between 2 and 4 tests for each type is found. Figure 27 neatly represents the laboratory experiment. Dahl then went on to present graphs which compare the CAI with AVS and AV, presented in figure 28.

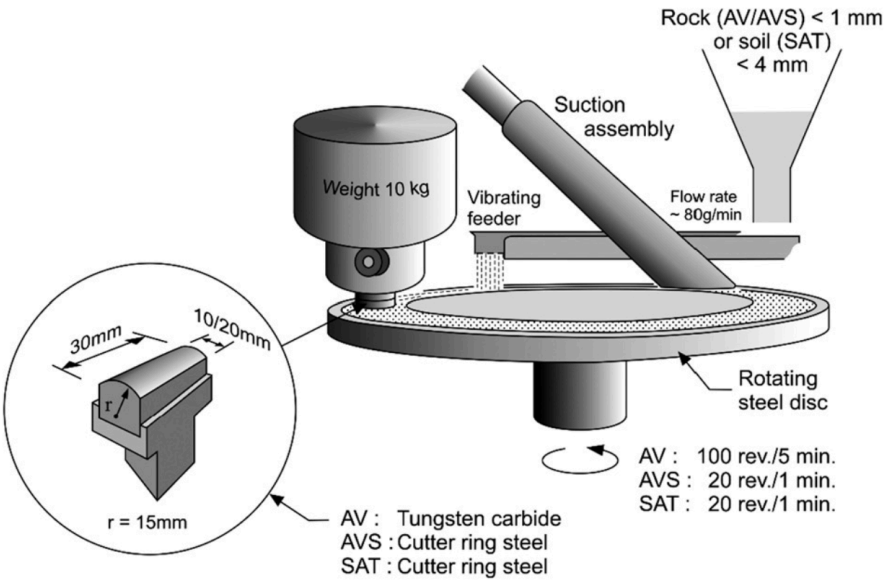

Figure 27: AV and AVS test. Adapted from Dahl et al. (2012)

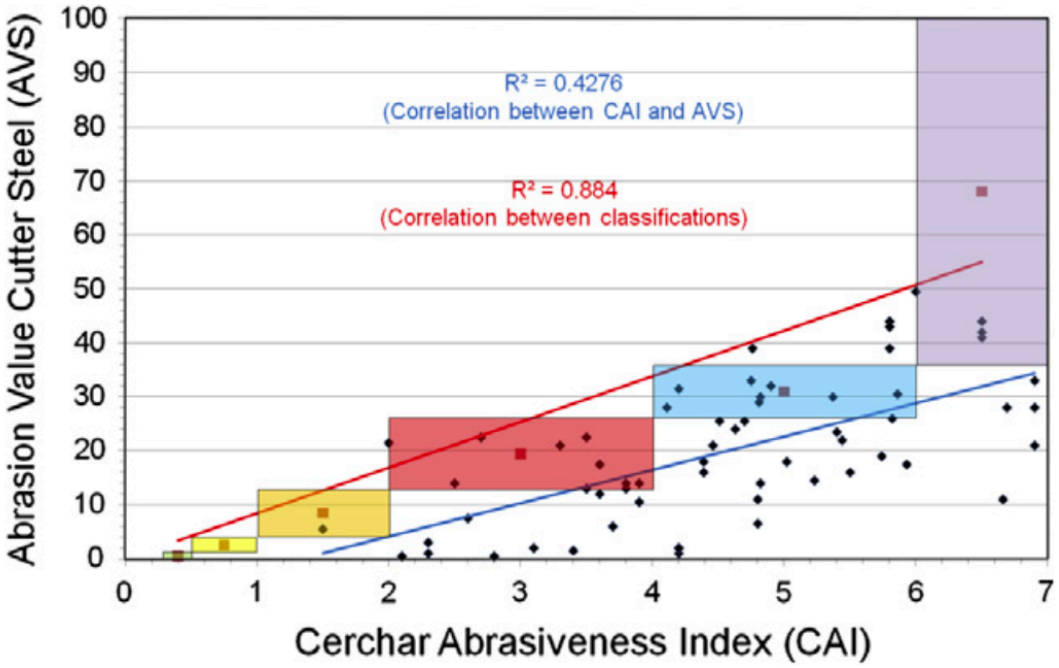

Figure 28: AV and CAI correlation. Adapted from Dahl et al. (2012)

As can be seen, this model relies heavily on a lot of empirical data, graphs and procedures, with the result being precise predictions. By making reference to the material provided by Bruland, it is possible to obtain all the crucial values.

The method

The Drilling Rate Index, DRI, value can be found using both the S_{20} and SJ values, easily summarised in Figure 29. Bruland was also able to develop equations for more accuracy, defining them as follows:

- When SJ < 50:

$$\text{DRI} = (0.13 \cdot SJ + 2.33) + S_{20}$$

- When SJ < 50:

$$\text{DRI} = \left[5.84 \cdot \ln(SJ) - 14\right] + S_{20}$$

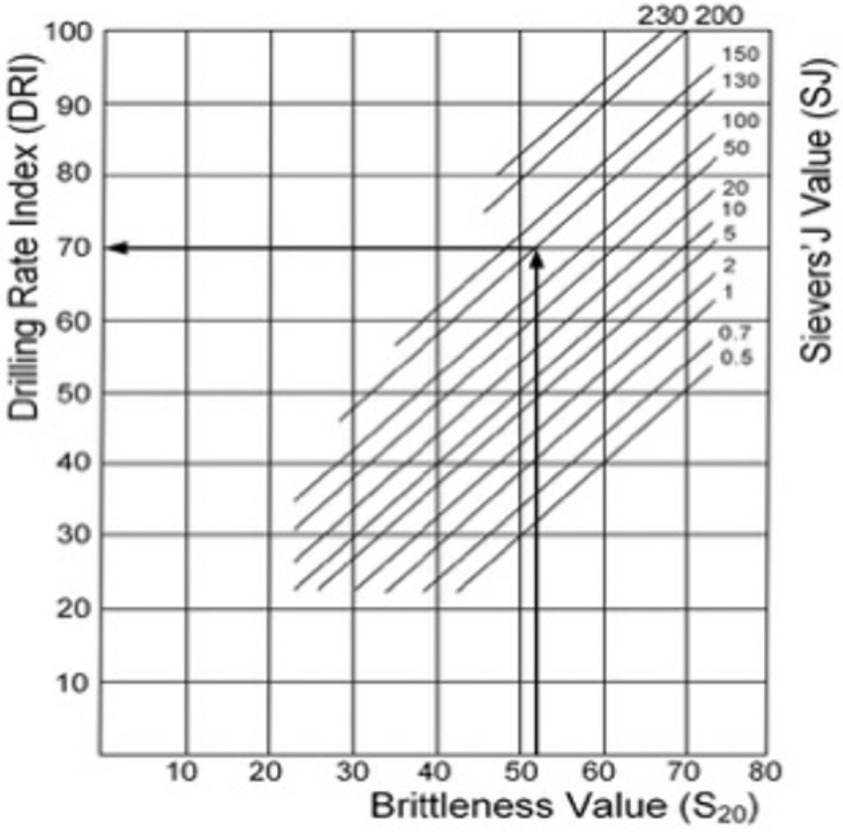

Figure 29: DRI assessment. Adapted from Bruland, (1998)

The author was also able to detail various DRI values for different rocks, providing Figure 30:

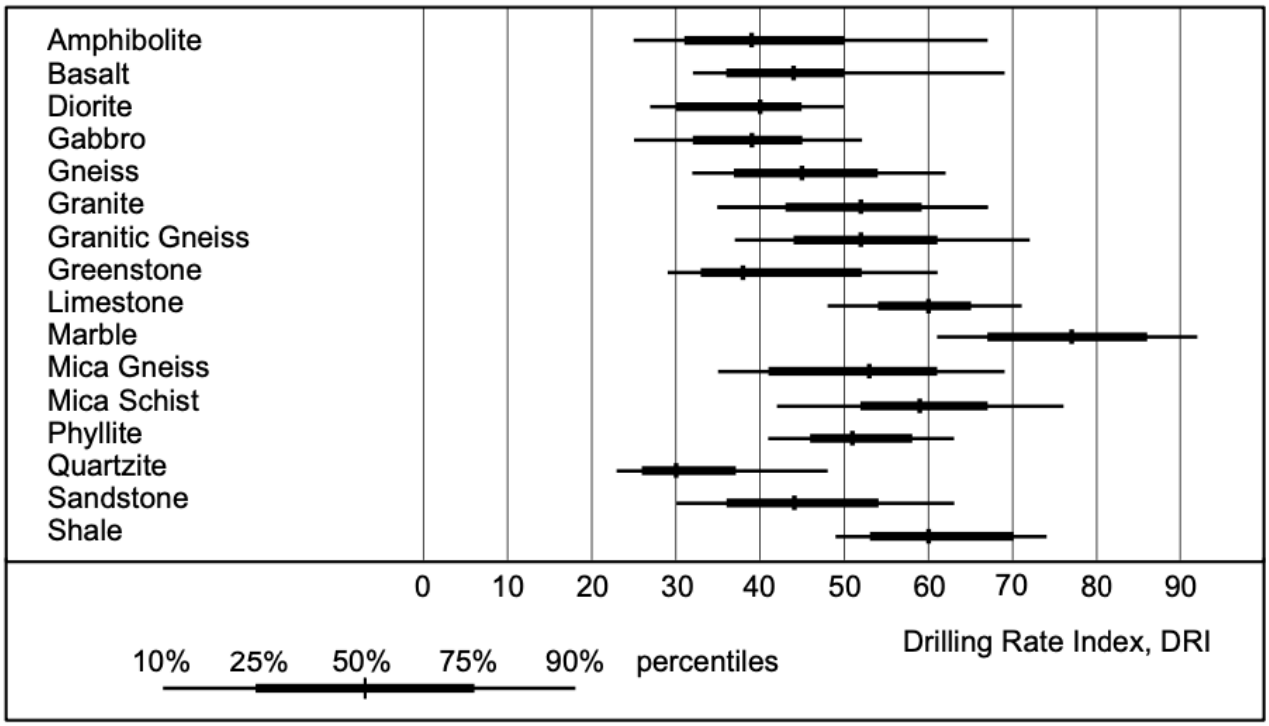

Figure 1.2 *Recorded Drilling Rate Index for some rock types. Data from* ***Project Report 13C-98 DRILLABILITY Statistics of Drillability Test Results.***

Figure 30: DRI variation for various rock types. Adapted from Bruland, (2000), figure 1.2

For the purposes of the program, it was decided to use the equations as these would provide a more precise result when compared to obtaining the value from the graphs. Functions were used to automatically select the correct equation based on the SJ value.

The Bit Wear Index, BWI, was also developed by Bruland by comparing the DRI and the AV. Quartz content was also found to have an effect. The diagram can be seen below in Figure 31.

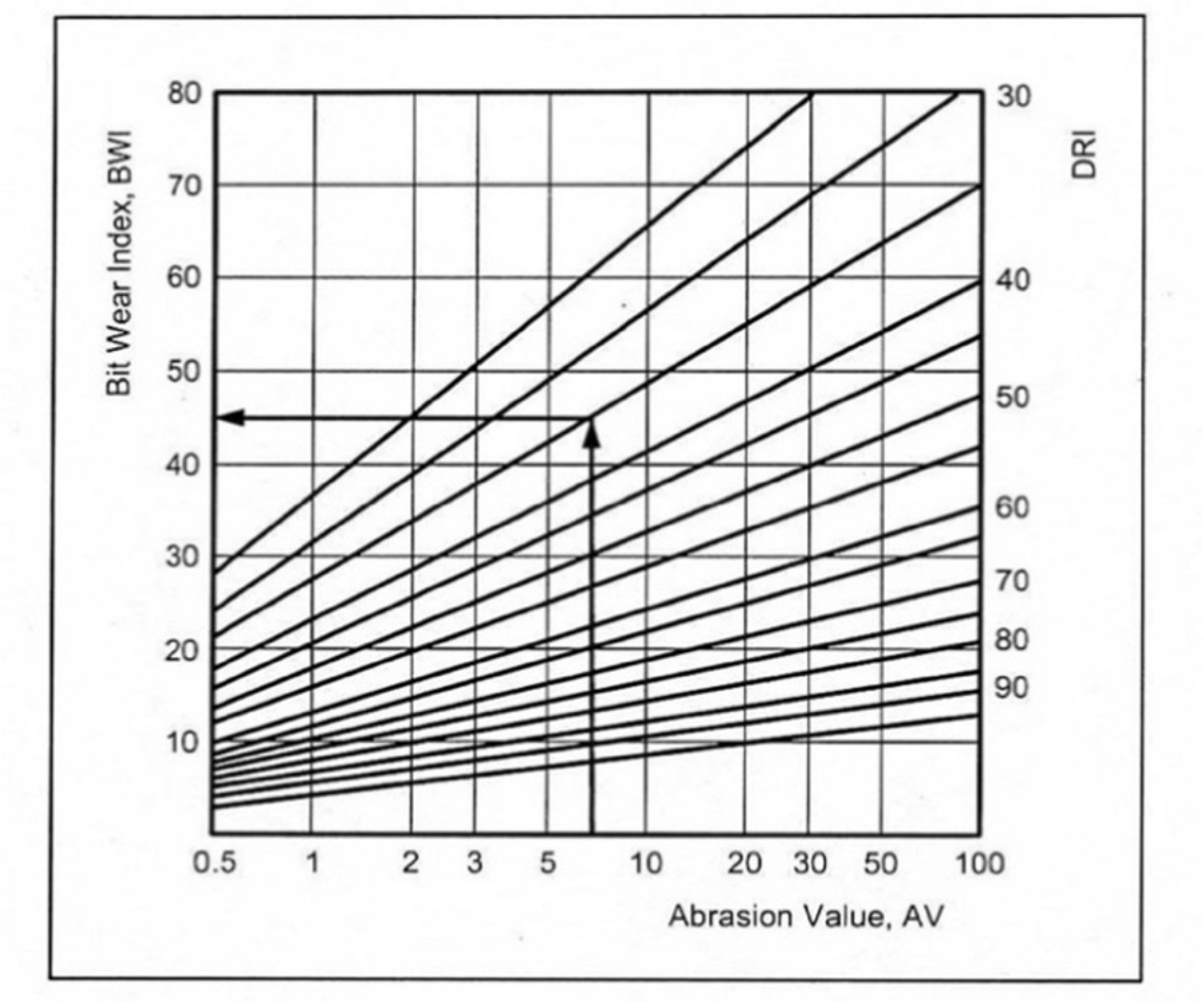

Figure 31: BWI assessment. Adapted from Bruland, (1998)

The Cutter Life Index, CLI, is also an important parameter that can be computed as follows:

$$\text{CLI} = 13.84 \cdot \left(\frac{SJ}{AVS} \right)^{0.3847}$$

Bruland found an updated calculation which was used in the program as all the input data was available, and is as follows:

$$\text{CLI} = 2.681 \cdot \text{CAI}^2 - 34.319 \cdot \text{CAI} + 111.09$$

Figure 32 was also compiled by Bruland to depict the CLI in terms of varying rock types.

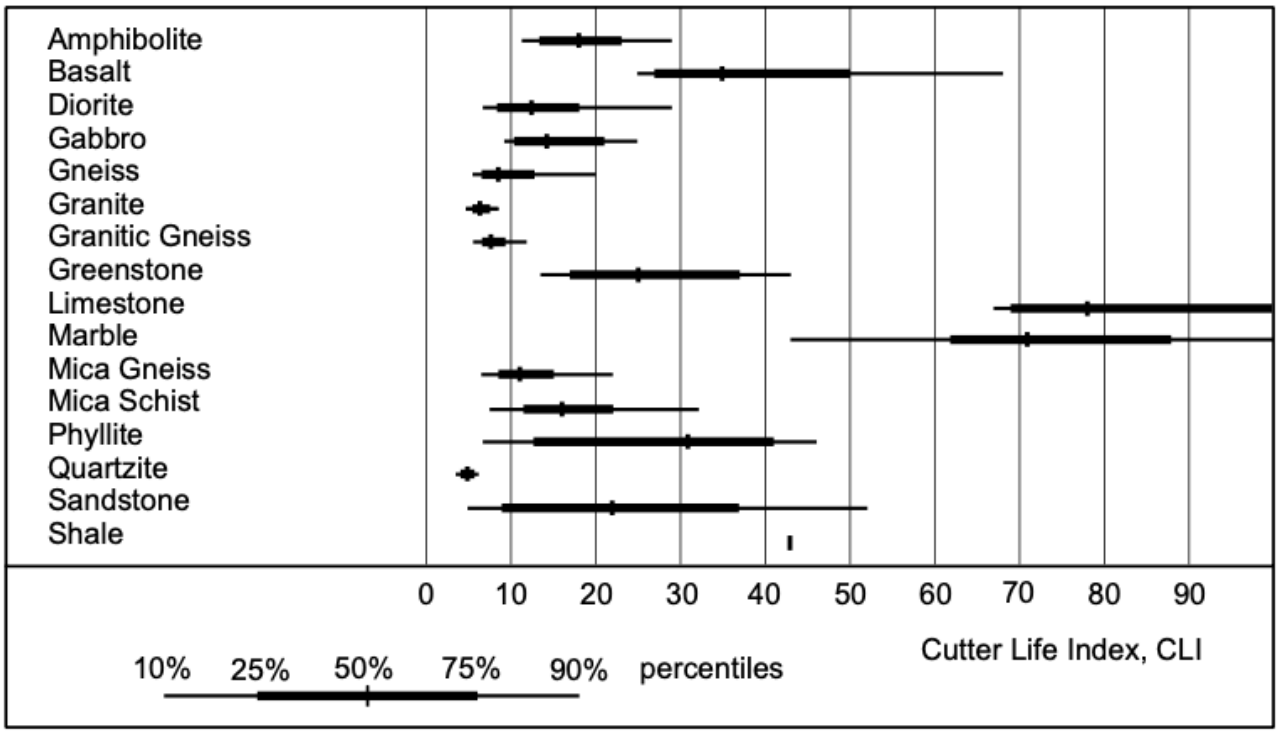

Figure 1.3 *Recorded Cutter Life Index for some rock types. Data from* ***Project Report 13C-98 DRILLABILITY Statistics of Drillability Test Results.***

Figure 32: CLI variation for some rock types. Adapted from Bruland, (2000), figure 1.3

The basic net penetration rate, in mm/rev, can be defined as:

$$i_0 = \left(\frac{M_{ekv}}{M_1} \right)^b$$

In which;

- M_{ekv}: gross thrust per cutter, kN
- M_1: critical thrust, kN (Essentially, it is the gross thrust per cutter needed for a 1mm penetration for every revolution of the cutterhead) and may be obtained from figure 33.
- b: penetration exponent, (It is a correction factor based on TBM and rock characteristics and may be obtained from figure 34.

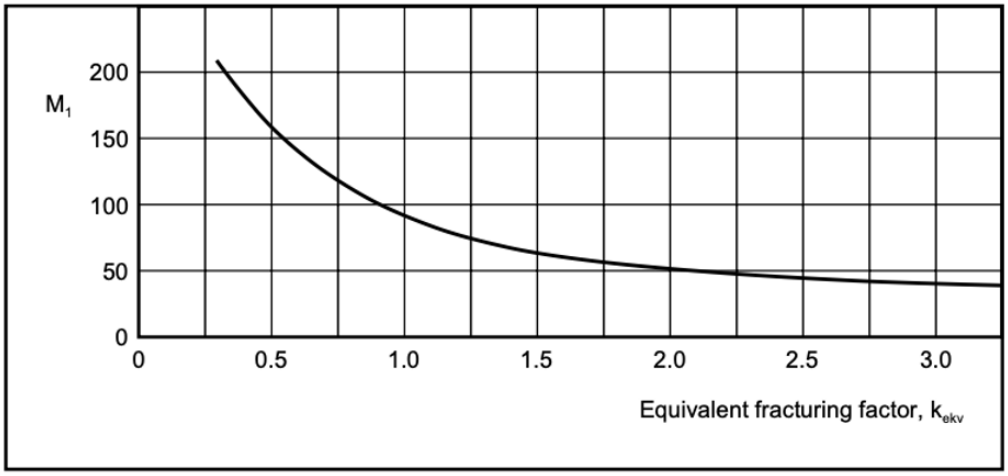

Figure 2.1 *Critical thrust as a function of the equivalent fracturing factor.*

Figure 33: Critical thrust from k_{ekv}. Adapted from Bruland, (2000), figure 2.1

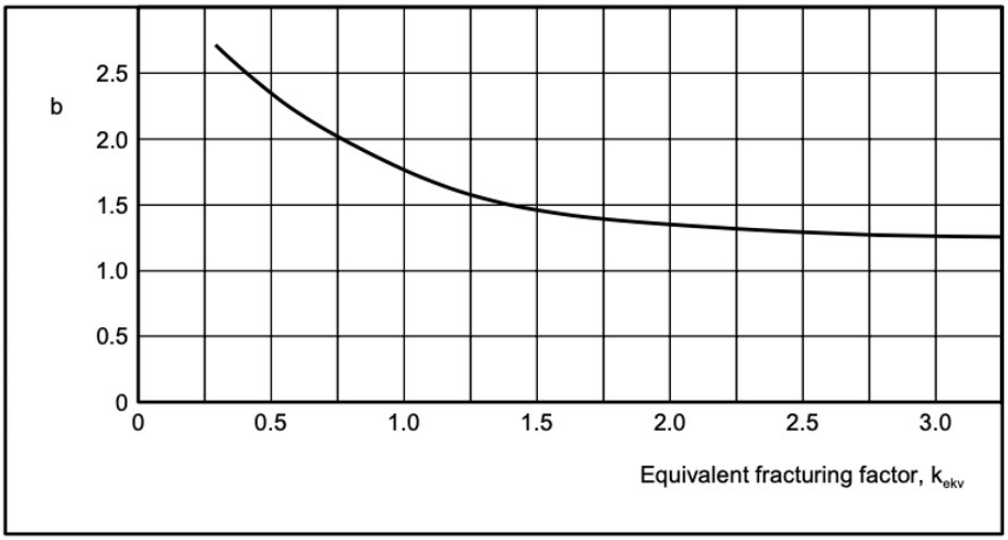

Figure 2.2 *Penetration coefficient as a function of the equivalent fracturing factor.*

Figure 34: Penetration exponent from k_{ekv}. Adapted from Bruland, (2000), figure 2.2

As can be seen, these graphs require that the equivalent fracturing factor k_{ekv}, is known. Alternatively, it is also possible to find the value of i_0 from a set of equations provided by Bruland in figure 35 or through the graph on figure 36. These equations also use k_{ekv} but can provide a more accurate result and this is why it was chosen to create a set of functions in the program that are capable of calculating i_0 based on the k_{ekv} value as well as the thrust on the disc. That being said, both methods were implemented into the program, and thus the operator is allowed to choose which method to use to obtain i_0.

Table 2.12 Equations for i_0 assessment

(kN/disc)		*Base penetration rate i_0 (mm/rev)*
100	$k_{ekv} < 1$	$-0.5208k_{ekv}^2 + 3.0521k_{ekv} - 0.8313$
	$k_{ekv} \geq 1$	$-0.36k_{ekv}^2 + 2.38k_{ekv} + 0.32$
150	$k_{ekv} < 1$	$-1.1489k_{ekv}^2 + 4.9531k_{ekv} - 1.2042$
	$k_{ekv} \geq 1$	$-0.4533k_{ekv}^2 + 2.96k_{ekv} + 0.0933$
200	$k_{ekv} < 1$	$-2.2825k_{ekv}^2 + 7.7135k_{ekv} - 1.4811$
	$k_{ekv} \geq 1$	$-0.3888k_{ekv}^2 + 2.814k_{ekv} + 1.524$
250	$k_{ekv} < 1$	$-5.5423k_{ekv}^2 + 13.522k_{ekv} - 2.3496$
	$k_{ekv} \geq 1$	$-0.3733k_{ekv}^2 + 2.92k_{ekv} + 3.0533$
300	$k_{ekv} < 1$	$-8.2721k_{ekv}^2 + 19.063k_{ekv} - 2.7904$
	$k_{ekv} \geq 1$	$-0.38k_{ekv}^2 + 2.91k_{ekv} + 5.47$

Source: Bruland (1998).

Figure 35: Equations pertaining to i_o. Reproduced from P. Grasso et al. (2023), table 2.12, originally by Bruland, (1998)

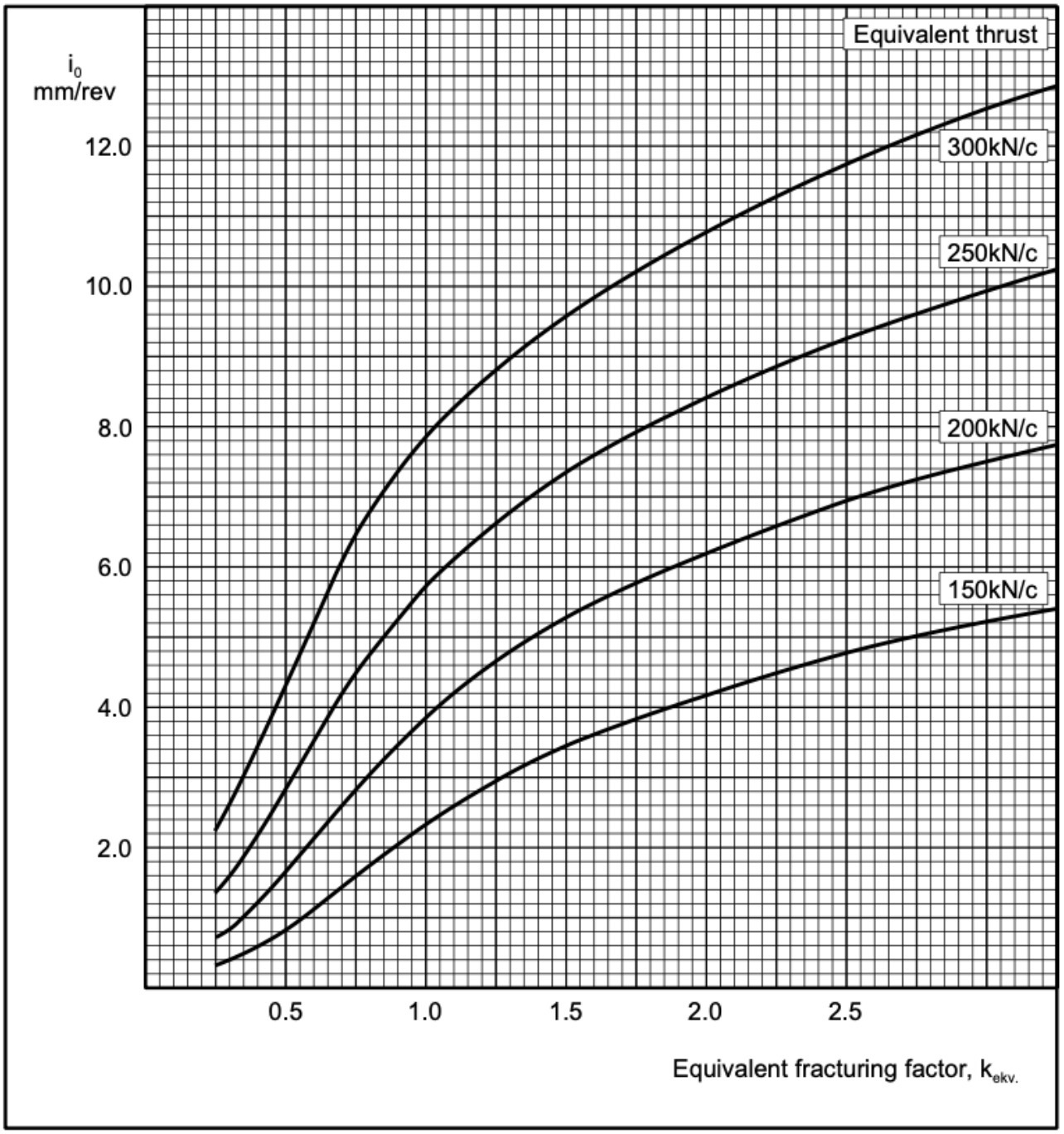

Figure 2.5 *Basic penetration. d_c = 483 mm and a_c = 70 mm.*

Figure 36: Graph to obtain i_o. Adapted from Bruland, (2000), figure 2.5

The values of M_{ekv} are k_{ekv} are needed to perform the initial portion of the calculations and thus the procedure to obtain these values, and their constituent equations is explained in the following categories as follows:

The equivalent fracturing factor, k_{ekv}

The equivalent fracturing factor, k_{ekv}, must be found by considering the rock weakness plane and the tunnel axis, specifically the angle between them, denoted by α. The k_{ekv} also utilises the rock mass fracture degree, thereby incorporating joints and fissures which have their own classification and are tabulated in figure 37. The angle α can be found via the following equation:

$$\alpha = \left| \arcsin\left(\sin\left(\alpha_F\right) \cdot \sin\left(\alpha_t - \alpha_s\right) \right) \right|$$

Where;

- α: angle between tunnel axis and joints
- α_f: plane of weakness dip angle
- α_t: tunnel axis direction
- α_s: planes of weakness strike angle

This is repeated for every fracture set present, and in the case of the program, it caters for up to 3 fracture sets. These values can then be used to compute the total fracturing factor.

Table 2.10 Fracture classes for both joints and fissures

Fracture class	*Spacing J_s (cm)*	*Classes with regard to J_s (cm)*
0	–	>240
0+	190	160–240
0–I	140	110–160
I–	90	60–110
I	40	7.5–60
I+	35	32.5–37.5
I–II	30	27.5–32.5
II–	25	22.5–27.5
II	20	17.5–22.5
II–III	15	12.5–17.5
III	10	8.75–12.5
III–IV	7.5	6.25–8.75
IV	5	4–6.25

Source: Bruland (1998).

Figure 37: Fracture classes. Reproduced from P. Grasso et al. (2023), table 2.1, originally by Bruland, (1998)

The program allows for the input of these fracture classes to automatically select the appropriate data for the rest of the equations pertaining to correction factor $k_{s,i}$.

Each value of α has a corresponding $k_{s,i}$ value, which may be calculated based on fracture or joint class from the following table as proposed by Bruland (1998) in figure 38:

Table 2.11 Equations for $k_{s,i}$ assessment

FC	JC	Correction factor $k_{s,i}$	
		$\alpha < 40°$	$40° < \alpha < 90°$
0	0	0.36	0.36
I	0–I	$0.0133\alpha + 0.45$	$-0.0005\alpha^2 + 0.0564\alpha - 0.4901$
II	I	$0.0158\alpha + 0.75$	$-0.0005\alpha^2 + 0.0586\alpha - 0.1196$
II–III	I–II	$0.017\alpha + 0.93$	$-0.0005\alpha^2 + 0.0576\alpha + 0.1291$
III	II	$0.02\alpha + 1.16$	$-0.0007\alpha^2 + 0.0835\alpha + 0.2894$
III–IV	II–III	$0.0248\alpha + 1.63$	$-0.0005\alpha^2 + 0.0622\alpha + 0.8789$
IV	–	$0.0243\alpha + 2.37$	$-0.0003\alpha^2 + 0.0483\alpha + 2.1246$

Source: Bruland (1998).

Figure 38: $k_{s,i}$ equations. Reproduced from P. Grasso et al. (2023), table 2.11, originally by Bruland, (1998)

In terms of the implementation of the method to obtain $k_{s,i}$, the equations of figure 38 were used as this provided an efficient way of obtaining accurate and valid results.

As mentioned previously, several fracture sets (or joint values) may be present, in which case, the following equation is used to obtain the total fracturing factor and is automatically calculated by the excel program:

$$k_{s,tot} = \left(\sum_{i=1}^{n} k_{s,i} \right) - (n-1) \cdot 0.36$$

Where:
- $k_{s,tot}$: total fracturing factor
- $k_{s,i}$: fracturing factor for set i, using figure 38
- n: number of fracturing sets

The DRI correction factor k_{DRI} can then be found either via the following equations or from figure 39. It is worth mentioning that the value k_{DRI} is dependant on the value of $k_{s,tot}$, and it being within certain boundaries:

- When $k_{s,tot} = 0.3$:

$$k_{DRI} = -0.0001\text{DRI}^2 + 0.0247\text{DRI} + 0.0293$$

- When $k_{s,tot} \geq 2$:

$$k_{DRI} = -0.00007\text{DRI}^2 + 0.0134\text{DRI} + 0.51$$

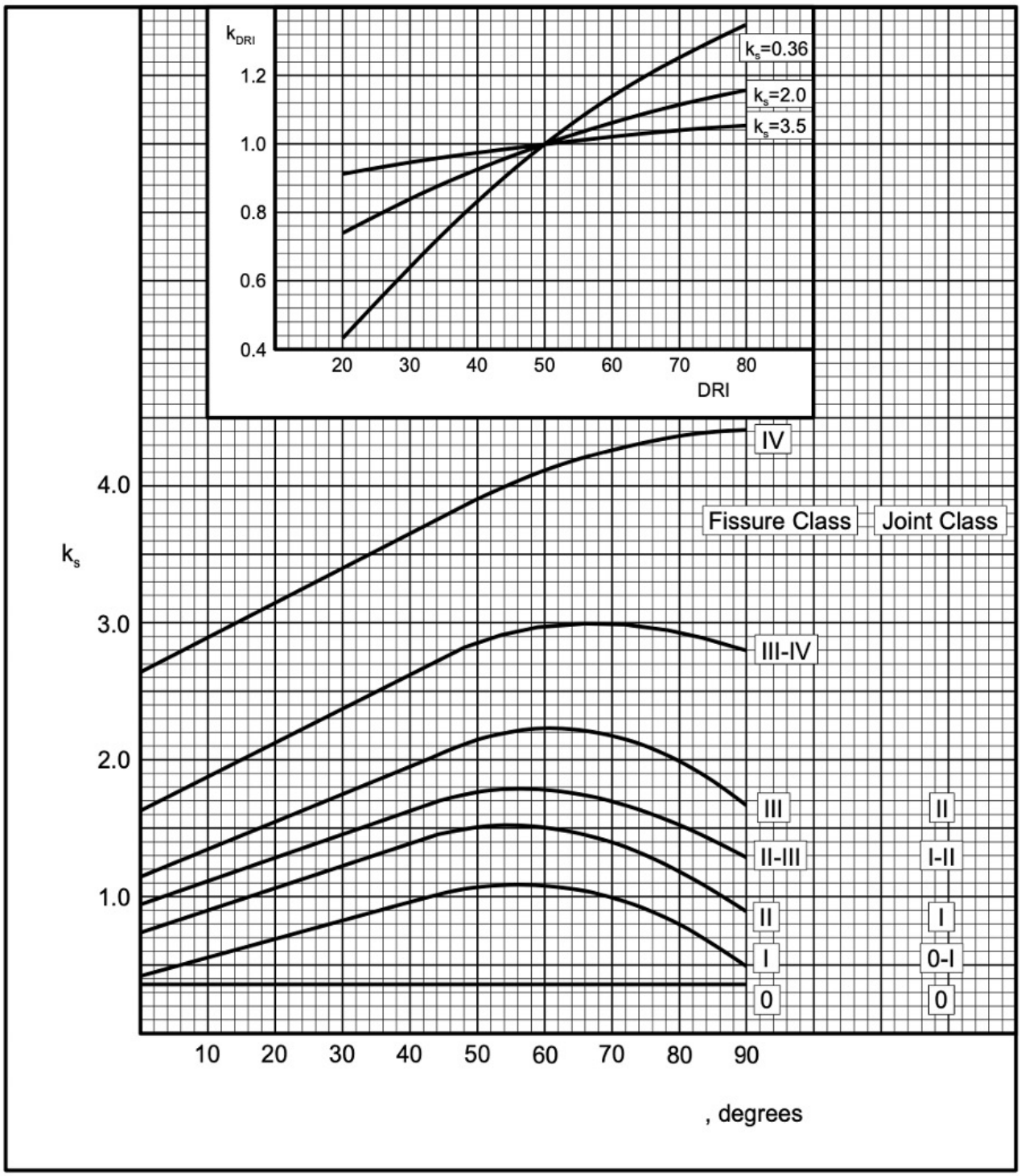

Figure 2.3 *Fracturing factor. Correction factor for DRI ≠ 50.*

Figure 39: Fracturing factor and DRI correction factor. Adapted from Bruland, (2000), figure 2.3

A function was implemented to obtain the best fitting value when $k_{s,tot}$ is between 0.3 and 2, as from the literature there is no direct method to deal with this and thus the conservative option is chosen with a midpoint value. Once more, the program is capable of selecting the appropriate equation for k_{DRI} based on the value of $k_{s,tot}$.

The rock porosity also has a relevant correction factor, denoted as k_{por}, the value of which can be taken from the following graph in Figure 40.

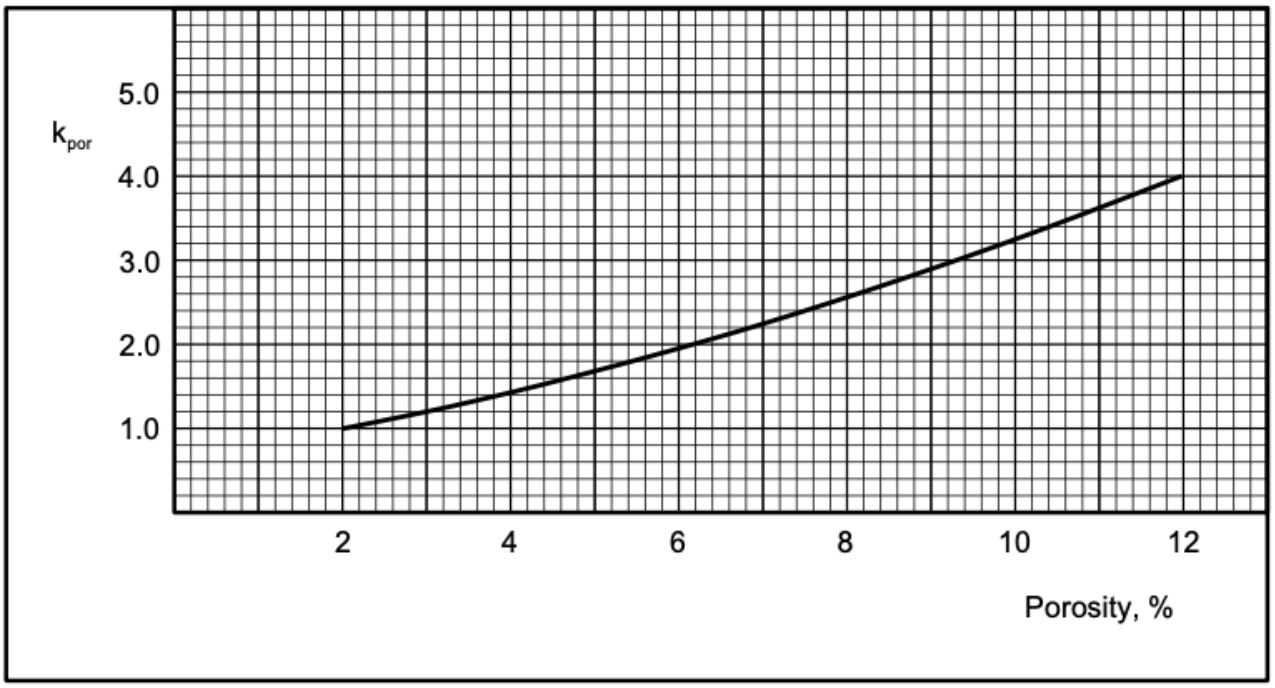

Figure 2.4 *Influence of rock porosity on the equivalent fracturing factor.*

Figure 40: Porosity correction factor. Adapted from Bruland, (2000), figure 2.4

No equations were present to obtain the porosity factor, so a polynomial equation was created that best fit the curve based on a few selected points. The coefficient of determination was also obtained and indicated that the equation is very precise. This is shown in figure 41:

Porosity factor - Figure 2.4	
Porosity [%]	**k_por**
2	1
4	1.4
6	1.95
8	2.59
10	3.21
12	4

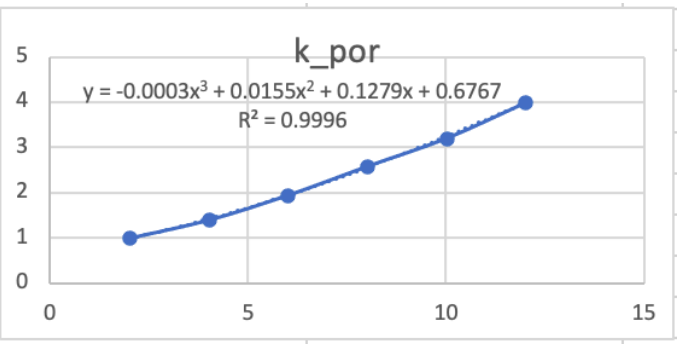

Figure 41: Re-graphed scheme to obtain necessary equations

Finally, k_{ekv} can be computed as:

$$k_{ekv} = k_{s,tot} \cdot k_{DRI} \cdot k_{por}$$

The equivalent thrust, M_{ekv}

This value is expressed as the product of the two correction factors for cutter diameter and average cutter spacing, k_d & k_a respectively, and the average gross thrust per cutter, M_B. Figures 42 and 43 can be used to obtain the correction factors, alternatively the corresponding equations are as follows:

$$k_d = 1 + 0.05 \cdot \frac{484 - \Phi_{disc}}{176}$$

$$k_a = 1 - 0.05 \cdot \frac{s_{cutters} - 69}{11}$$

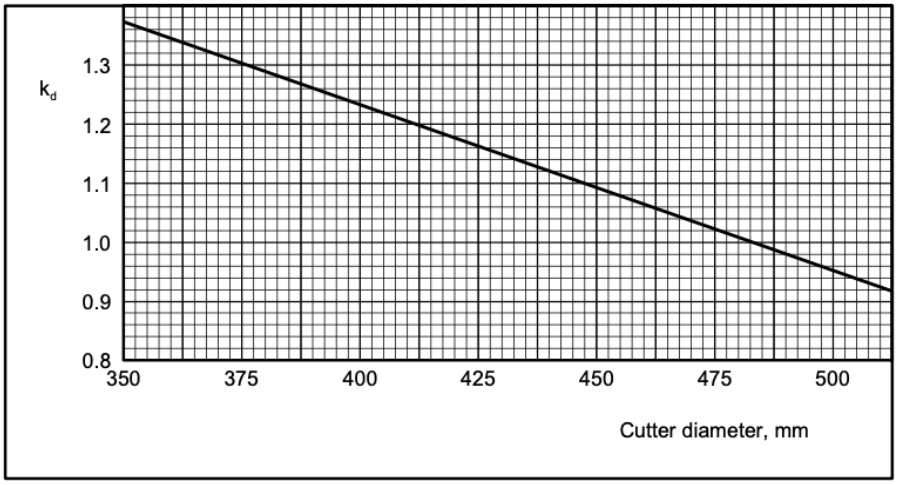

Figure 2.6 *Correction factor for cutter diameter $d_c \neq 483$ mm.*

Figure 42: Cutter diameter correction factor. Adapted from Bruland, (2000), figure 2.6

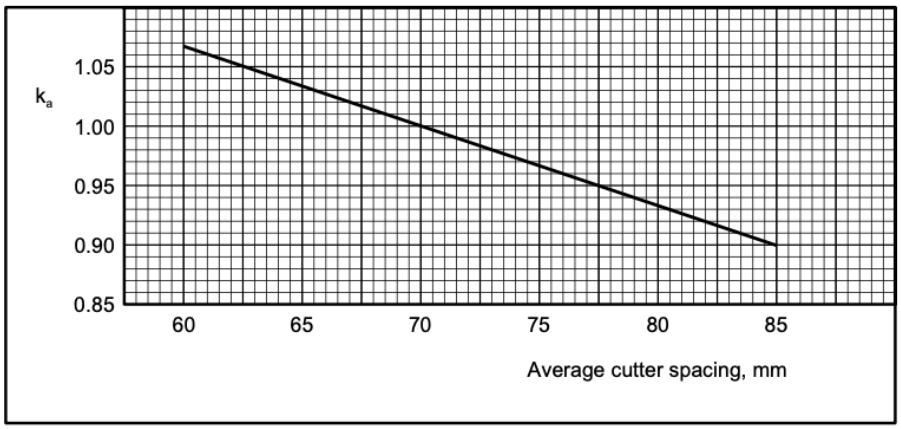

Figure 2.7 *Correction factor for average cutter spacing $a_c \neq 70$ mm.*

Figure 43: Cutter spacing correction factor. Adapted from Bruland, (2000), figure 2.7

Once more, the equations were used to obtain these factors.

M_B is found by dividing the reduced axial thrust of the machine by the total number of cutters. The final equation is therefor:

$$M_{ekv} = M_B \cdot k_d \cdot k_a$$

Finally, it is possible to find the base penetration rate can be computed with the previous equation:

$$i_0 = \left(\frac{M_{ekv}}{M_1} \right)^b$$

Or as explained before, via the numerical approach or from figure 36.

In the case of the excel program, it was decided to utilise the equations in figure 29 to provide accurate results - it is possible to find the i_o value through the relevant k_{ekv} by interpolation, in the case where the force per cutter disk is not exactly as those listed in the table. These values can also be plotted as they are essentially the equations that define the graph in figure 36.

The next step would be to identify the correct rolling velocity, v_{cutter}, for the relevant cutter size, the most common of which have been reported hereunder:

Φ_{disc}		**v_{cutter}**
“	**mm**	**ms^{-1}**
19	483	2.62
17	432	2.3

It will then be possible to compute the net penetration rate, defined as ROP_0, through the following calculation and is given in meters per hour:

$$ROP_0 = I_0 = i_0 \cdot v_{rot} \cdot \left(\frac{60}{1000} \right)$$

Cutter wear:

As the cutters are responsible for the excavation, their life span is influenced by various parameters, which have an effect on the total wear of the cutters. The most notable variables are listed by Bruland in figure 44.

Table 2.13 Parameters influencing the net penetration rate

Rock mass parameters	*Machine parameters*
Rock type abrasiveness	Cutter diameter
Quartz content	Cutter type and quality
Porosity	Cutterhead diameter and shape
	Rotational speed of the cutterhead
	Number of cutters on the cutterhead

Source: Bruland (1998).

Figure 44: Net penetration rate influence parameters. Reproduced from P. Grasso et al. (2023), table 2.13, originally by Bruland, (1998)

The equation that takes these factors into account provides the average cutter ring life in h/cutter, and is as follows:

$$H_h = \frac{H_0 k_\Phi k_Q k_{RPM} k_N}{N_{TBM}}$$

Where:

H_0 is defined as being the basic ring life of the cutter. This can either be found from figure 45, or through the following equations, which depend on the cutter diameter and the CLI calculated previously.

For a 17” cutter:

$$\text{CLI} < 30, \Rightarrow H_0 = -0.0925\text{CLI}^2 + 6.1657\text{CLI} + 0.65$$
$$\text{CLI} \geq 30, \Rightarrow H_0 = -0.0044\text{CLI}^2 + 1.3333\text{CLI} + 67.5$$

For a 19” cutter:

$$\text{CLI} < 30, \Rightarrow H_0 = -0.1425\text{CLI}^2 + 8.305\text{CLI} + 1.05$$
$$\text{CLI} \geq 30, \Rightarrow H_0 = -0.0031\text{CLI}^2 + 1.2483\text{CLI} + 88.75$$

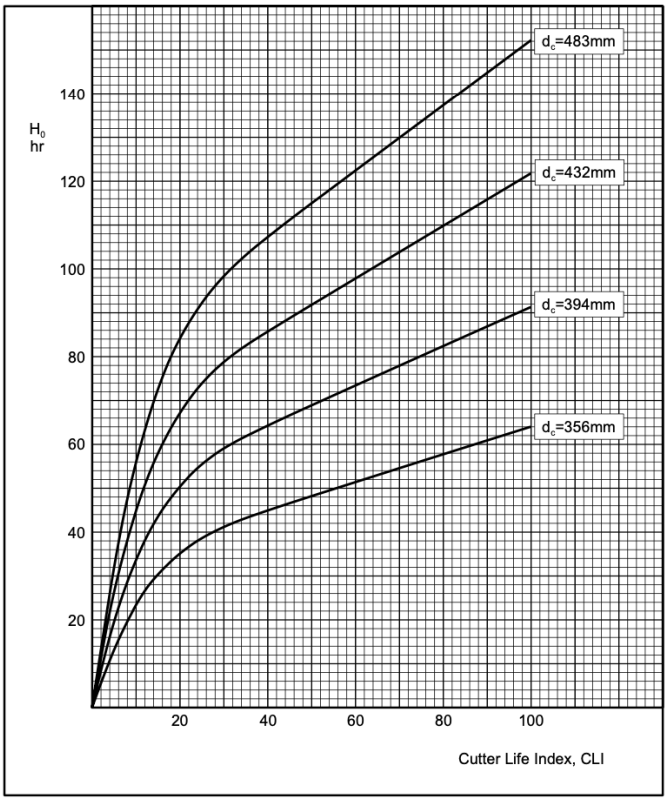

Figure 3.1 *Basic cutter ring life, H_0 .*

Figure 45: The basic cutter ring life, H_0.
Adapted from Bruland, (2000), figure 3.1

As in previous instances, the equations were opted for over picking points on the graph for the sake of greater precision in final values. The program uses the correct equation depending on the cutter size which is an input function, and the CLI from the previous calculations.

A correction factor for the cutterhead shape and diameter is needed and is given by k_Φ. Its value can be taken either from figure 46, or calculated with the following equation (as used by the program):

$$k_\Phi = -0.0065\Phi_{TBM}^2 + 0.2061\Phi_{TBM} + 0.474$$

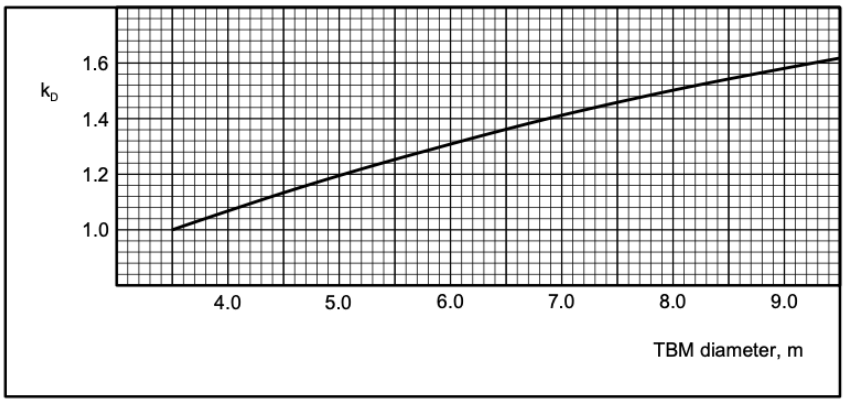

Figure 3.2 *Correction factor for TBM diameter.*

Figure 46: TBM diameter correction factor. Adapted from Bruland, (2000), figure 3.2

The quartz content correction factor is given by k_Q. It is important as it factors in the abrasiveness of the rock depending on its type, as explained by figure 47. The following equations can also be used for a numerical approach and provide a more precise result, hence why they were used in the program:

For q < 0.27:

$$k_Q = -0.00009q^2 + 0.004q + 0.6\,(\pm 0.08)$$

Any other value of q:

$$k_Q = 0.00009q^2 - 0.0196q + 1.714\,(\pm 0.08)$$

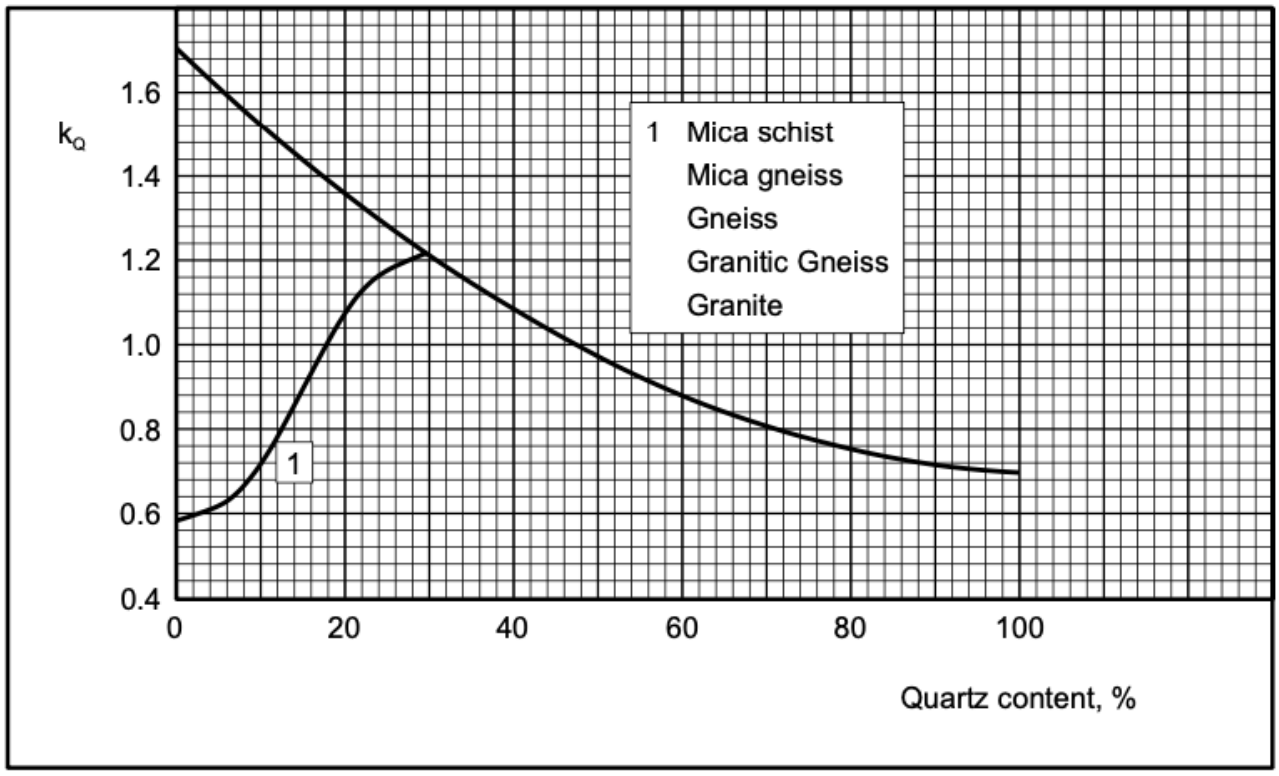

Figure 3.3 *Correction factor for rock quartz content.*

Figure 47: Quartz content correction factor. Adapted from Bruland, (2000), figure 3.3

As the equations were used, another function was also made to choose the correct equation depending on the quartz content value which is a known input value.

The cutterhead rotation speed correction factor is k_{RPM} and utilises the average TBM rotation speed based on its diameter, via figure 48. The equation is given by:

$$k_{RPM} = \frac{50}{\Phi_{TBM} \cdot v_{rot}}$$

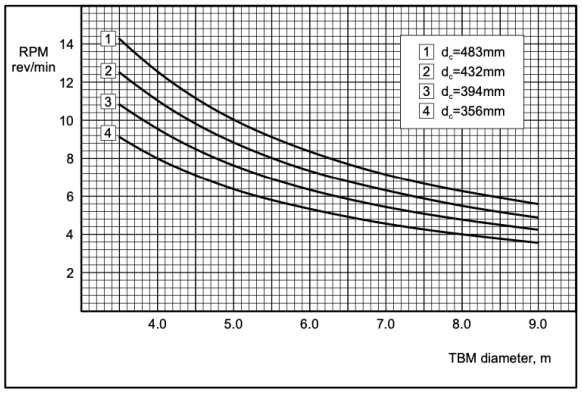

Figure 1.5 *Cutterhead rpm.*

Figure 48: Cutterhead RPM. Adapted from Bruland, (2000), figure 1.5

For desired precise results, the equation was used in the program, which is based on already known parameters set by the manufacturer.

The last correction factor is k_N for the number of cutter discs, and is obtained through the following equation in which N_{TBM} is the number of cutter disks.

$$k_N = \frac{N_{TBM}}{N_0}$$

where N_0 is given by the equation below or figure 49. The cutter spacing is denoted by $s_{cutters}$.

$$N_0 = \frac{\Phi_{TBM}}{2 \cdot s_{cutters}}$$

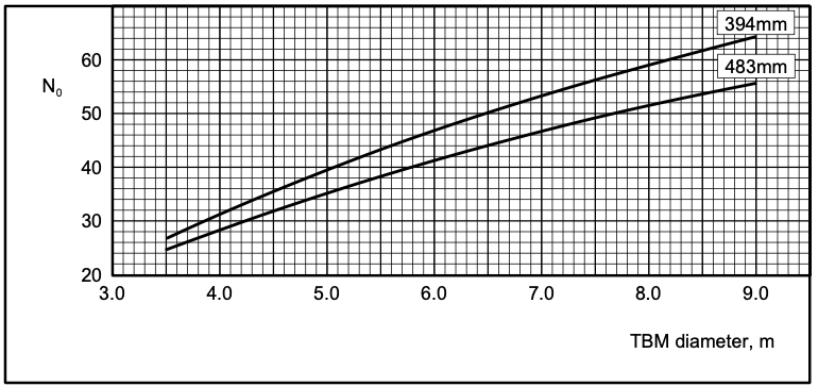

Figure 1.6 *Normal number of cutters on the cutterhead.*

Figure 49: Average number of cutters. Adapted from Bruland, (2000), figure 1.6

In this case, the equation given results in the value of N_0 being equal to 1 which is not appropriate as a correction factor. Therefor, figure 49 was used to create a set of equations based on the known points from the graph. These equations are in the form of polynomials and were chosen as the best fit for the curves. The coefficient of determination was also found, indicating the goodness of the equations. These were then used to compute the correct value of N_0. Figures 50 and 51 represent this:

Average number of cutters - Figure 1.6		
X (TBM_d meters)	394mm, 15 inch N_0, 394mm	483mm, 19 inch N_0, 483mm
3		
3.5	27	25
4	31	28
4.5	35	32
5	39.5	35
5.5	43	38
6	47	41
6.5	50	44
7	53.5	47
7.5	56.25	49
8	59	51.5
8.5	61.8	53.5
9	64	55.5
9.5		

	cutter diamter	N_0
Avg. no. cutters	15	31.1353
Avg. no. cutters	17	29.7353
Avg. no. cutters	19	28.3353

Figure 50: Average number of cutters computation

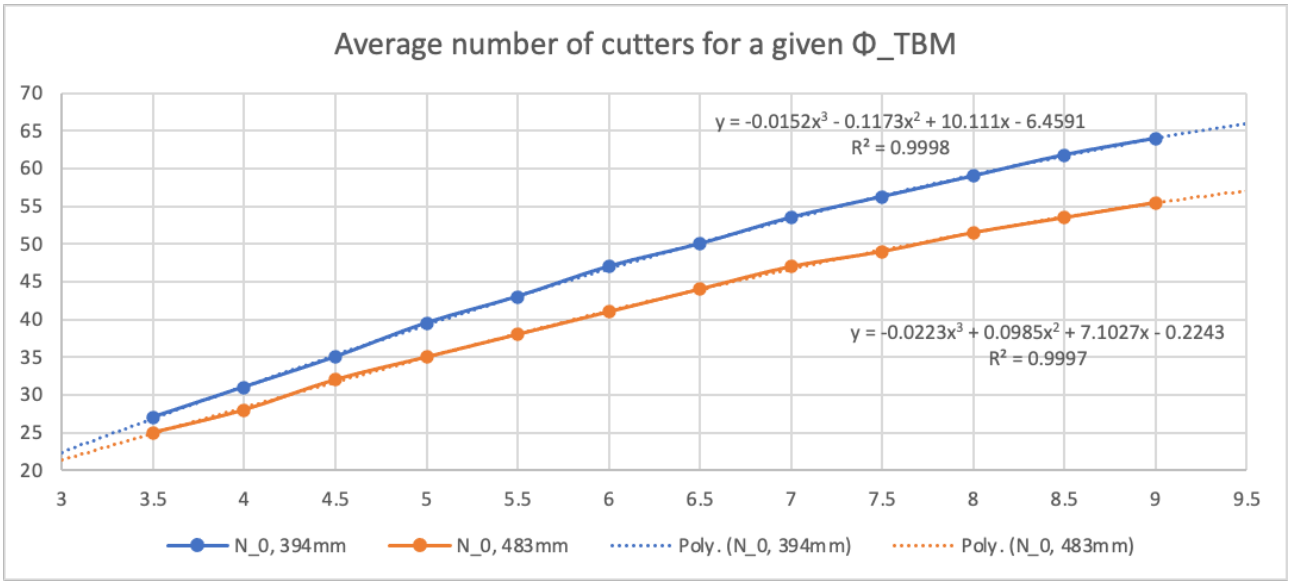

Figure 51: Re-graphing scheme to obtain necessary equations

It is then possible to obtain the cutter ring life from the following equation. This value will be in m^3/cutter.

$$\text{CRL} = i_0 \cdot H_h \cdot \frac{\Phi_{TBM}^2 \cdot \pi}{4} \cdot \frac{v_{rot} \cdot 60}{1000}$$

A final step would be to identify the net and gross excavation times. For the net excavation time, the value is expressed in hours by dividing the total planned tunnel length in meters by the net penetration, ROP_0, in meters per hour. Dividing this final value by 24 will provide the net excavation time in terms of days.

The gross excavation time is then found by dividing the net excavation time by a machine utilisation coefficient in the range of 0.4 to 0.5. this is to account for machine stoppage times.

4.22 Alber 1996 model

A model was proposed by Prof. Alber in 1996 with Ruhr University, Bochum. This model relies on the uniaxial rock mass strength as we all as the failure criterion of Hoek-Brown. Albers conducted analysis on 110km of tunnelling in which five TBMs were used and summarised in table 4. The main rock types encountered were sandstone, limestone, mudstone, dolomitic shale, dolostone, shale, dolerite, and basalt. Mylonit was also reported in faults.

Parameter	Unit	Low Value	High Value
σ_c	MPa	20	320
σ_{cm}	MPa	1	160
Φ_{TBM}	m	2.9	6.6
Φ_{disc}	Inches	15	19
v_{rot}	rpm	2.3	10

Table 4: Excavation parameters. Adapted from Alber, (1996)

A relationship between the geology and performance parameters was determined and is expressed as:

$$SE = \frac{\sigma_{cm}}{\sigma_\theta} = \frac{\sigma_{cm}}{\sigma_v \cdot \left(3k - 1\right)}$$

Using:

$$\sigma_{cm} = \sigma_c \sqrt{s}$$

$$s = exp\left(\frac{RMR_{TBM} - 100}{9}\right)$$

$$RMR_{TBM} = 0.84 \cdot RMR + 21$$

$$v_s = 0.74 \cdot \left(CAI_{mod}\right)^{1.93}$$

$$\sigma_m = \frac{\sigma_v + 2\sigma_\Theta}{3}$$

In which:

- SE: Stability Estimate
- σ_θ: tangential stress via the Kirsch equation
- σ_{cm}: uniaxial rock mass strength
- v_s: specific ring weight loss, mg/m

The specific penetration, SP, can also be found from figure 52:

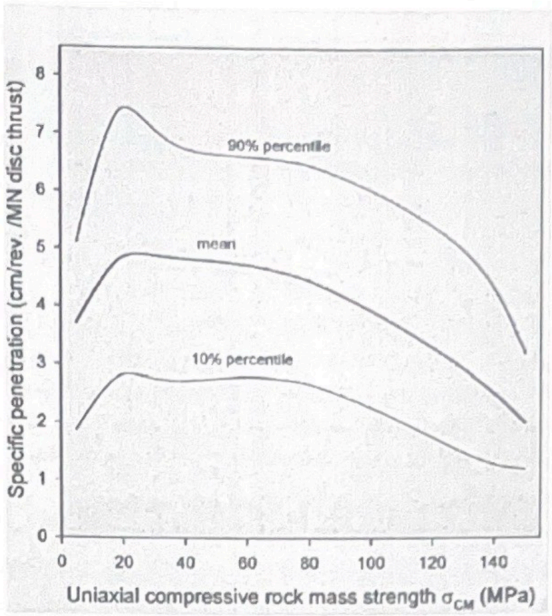

Figure 2.54: *SP as a function of σ_{cm}, 17 inches discs, Alber*

Figure 52: SP. Adapted from Alber, (1996), figure 2.54

For every other case when the rock mass strength is less than 20MPa, the SP decreases when σ_{cm} does too. This is usually because the rock mass becomes increasingly weaker and more fractured at low σ_{cm} values. Figure 53 was then used to show the relation between CAI and the stress

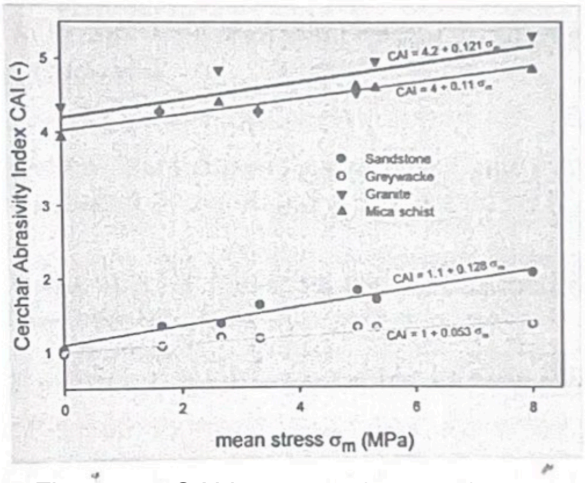

Figure 53: CAI in terms of state of stress. Adapted from Alber, (1996)

4.23 Alvarez Grima 2000 model

Grima et al. were the first to develop a neuro-fuzzy model for the performance prediction of TBMs. In this particular model, specific equations are used when certain conditions are satisfied for data clusters. The Core Fracture Frequency, CFF, which is also the inverse of J_s, is used:

$$ROP_1 = -0.72 \cdot CFF - 0.01 \cdot \sigma_c + 0.1 \cdot v_{rot} + 0.001 \cdot F_N + 0.006 \cdot \Phi_{disc} + 0.93$$

$$ROP_2 = -1.95 \cdot CFF - 0.05 \cdot \sigma_c + 0.13 \cdot v_{rot} + 0.03 \cdot F_N + 0.04 \cdot \Phi_{disc} - 24.65$$

$$ROP_3 = -9.63 \cdot CFF - 0.13 \cdot \sigma_c + 3.33 \cdot v_{rot} + 0.05 \cdot F_N - 0.009 \cdot \Phi_{disc} + 1.31$$

$$ROP_4 = -1.45 \cdot CFF - 0.06 \cdot \sigma_c + 1.94 \cdot v_{rot} + 0.35 \cdot F_N - 0.26 \cdot \Phi_{disc} - 8.08$$

Grima et al. then proposed a weighted function, in which w_i represent the weight functions:

$$ROP = \frac{w_1 \cdot ROP_1 + w_2 \cdot ROP_2 + w_3 \cdot ROP_3 + w_4 \cdot ROP_4}{w_1 + w_2 + w_3 + w_4}$$

4.24 Yagiz 2008 model

In 2008, Yagiz et al. created a model developed on the number 3 Queens Water Tunnel, in New York, which is 7.5km in length. A TBM with a 7.06m diameter and 19 inch disc cutters was used. It was reported that the geological composition was of mainly metamorphic igneous rock, with a compressive strength between 110 MPa and 210 MPa. The author also implemented a parameter to account for rock brittleness and denoted it as the Peak Slope Index, PSI, which is the ratio of the maximum load and displacement and is expressed in kN/mm.

$$PSI = \frac{F_{max}}{u_{max}} = \frac{\sigma_c \cdot A}{\epsilon \cdot L} = E \cdot \frac{A}{L}$$

They also showed that the following equation can also be used:

$$PSI = 0.198 \cdot \sigma_c - 2.174 \cdot \sigma_t + 0.913 \cdot \rho \cdot g - 3.807$$

The penetration rate in m/hr is then as follows:

$$ROP = 1.093 + 0.029 \cdot PSI - 0.003 \cdot \sigma_c + 0.437 \cdot log\,(\alpha) - 0.219 \cdot J_s$$

In which:

- J_s is in meters
- σ_c is in MPa
- α is in °

4.25 Gong & Zhao 2009 model

An analysis was carried out on the Deep Tunnel Sewerage System in Singapore by Gong and Zhao in 2009. The 22.2km excavation was achieved via two EPB double-shield Herrenknecht machines. The largest machine was outfitted with a 4.88m diameter face, with 35 cutters at 100mm spacing. Various rock types were encountered, including both soft ground and rock.

Gong and Zhao deduced that the boreability of the rock could be found as follows, in which FPI_{1mm} is defined as the FPI at a penetration rate of 1mm per revolution:

$$FPI = FPI_{1mm} \cdot PR^{-0.75}$$

A non-linear analysis was then carried out with the respective equation as follows, the R^2 value is 0.75:

$$FPI_{1mm} = 37.06 \cdot \sigma_c^{0.26} \cdot BI^{-0.1} \cdot \left(0.84e^{-0.05 \cdot J_v} + e^{-0.09 \cdot sin(\alpha + 30)}\right)$$

Furthermore:

$$FPI = 37.06 \cdot \sigma_c^{0.26} \cdot BI^{-0.1} \cdot \left(0.84e^{-0.05 \cdot J_v} + e^{-0.09 \cdot sin(\alpha + 30)}\right) \cdot PR^{-0.75}$$

Issues exist in this model, mainly pertaining to the cutterrhead stress distribution, fixed lithology and machine parameters, and the fact that groundwater stress was not considered.

4.26 Hassanpour et al. 2011 model

The authors here based their model on data from a series of projects carried out in Iran and single one in New Zealand. Together, 56.4km were analysed. One open TBM and three double shield TBMs were used for the projects, with their diameters ranging between 4.53m and 10.05m. The compressive strength of the rock encountered ranged between 15MPa and 225MPa. Various rock types were also encountered such as limestone, sandstone, shale, quartzitic schist, phyllite, and many more.

Hassanpour et al.'s analysis revealed the following equation with a 0.785 regression coefficient:

$$FPI = exp\left(0.008 \cdot \sigma_c + 0.015 \cdot RQD + 1.384\right)$$

4.27 Farrokh et al. 2012 model

Farrokh et al. examined a collection of data from 17 projects that captured a cast range of conditions of the 73.6km excavated. In these projects, 6 doubled shields, 2 single shields, 7 open, 2 slurry and 2 mixed TBMs were used. Their diameters ranged between 3.84m and 11.8m and the rotation speed was between 6 and 11 rpm. Many rock types were also excavated through, such as limestone, quartzitic schist, gneiss and more.

The equation they developed has a an R^2 value of 0.63 and is as follows:

$$PR = exp\left(0.41 + 0.404 \cdot \Phi_{TBM} - 0.027 \cdot \Phi_{TBM}^2 + 0.0691 \cdot RT_c - 0.00431\sigma_c + 0.0902 \cdot RQD_c + 0.000893 \cdot F_N\right)$$

In which RT_c is the numerical code for that rock type in table 5, and RQD_c is the RQD code from table 6.

Rock type	Code	RT_c
Claystone, mudstone, marl, slate, phyllite, argilite	C	5
Sandstone, siltstone, conglomerate, quartzite	S	3
Limestone, chalk, dolomite, marble	L	3
Karsitic limestone	K	3
Metamorphic rocks such as gneiss and schist	M	2
Fine volcanic such as basalt, tuff and andesite	V	2
Coarse igneous such as granite and diorite	G	1

Table 5: Numerical rock type codes. Adapted from Farrokh et al. (2012)

Joint spacing J_s [cm]	RQD value	RQD_c value
> 12.5	100	1
8.5 - 12.5	0 - 90	2
6 - 8.5	≤ 60	3

Table 6: RQD values. Adapted from Farrokh et al. (2012)

4.28 The Excel file prediction model

The excel program was created to compare the output values of the main methods, NTNU model, CSM model, and Gehring model. The basic equations of the other mentioned methods were also included to produce a more comprehensive comparison. The file was split up into several workbooks to improve the user experience. Input parameters, whether they are general or specific to the method, were incorporated in this one workbook. This allows for quick amendments and data value input in a clear and concise manner.

Each prediction model then has its own workbook pertaining to the relevant calculations. This is where the actual method is programmed to obtain results. Various tables and figures proposed by the authors were used to help do this and the values and data were set up in such a way as to make them easier to follow, in line with the methods' procedure.

The outputs also have their own workbook. In this, all the output values are neatly organised for comparison between the different methods. The prediction models are listed with their relevant output parameters such as penetration, cutter excavation life, and excavation time. This is advantageous as an operator will be able to observe the data side by side and gain insight on what the most probable outcome is.

As previously explained, some equations were not available, however, their respective graphs from data were. In light of this, equations were made that best fit the graphs to be able to carry out numerical analysis. In all the cases, the R^2 values were relatively high, supporting accurate results.

5. Application

The main prediction models, NTNU and CSM, were tested against data used in an academic assignment alongside their hand calculation counterparts. The primary reason for comparing these two models in this way was because values for easy, average and hard conditions were provided, and there was the added advantage of being able to observe the difference between hand calculations and more rigorous numerical analysis. This would serve to provide a very interesting outlook in the differences between the results.

The easy, average and hard conditions were as follows:

Parameter	Easy	Average	Hard
CAI	3.4	3.67	4.1
S_{20} [%]	49.5	39.9	27.16
S_j [1/10 mm]	20	9	1.74

Table 7: Conditions

The rest of the conditions were described as follows:

Name	Parameter	Value	Unit
Tunnel length	L	5000	m
Maximum axial thrust	F_max	7440	kN
Reduced axial thrust	F_reduced	7070	kN
TBM diameter	⌀_TBM	4	m
Number of TBM cutters	N_TBM	31	#
TBM cutter diameter	⌀_cutter	17	“
Maximum cutter force	F_cutter, max	240	kN/cutter
Quartz content	q	45	%
Sub vertical schistosity	α_f	± 15	°
Joint spacing	J_s	50 - 100	mm

Table 8: Input parameters

This data was used in the input section of the excel program, and the outputs were recorded for every condition, for both the NTNU and CSM models. All the numerical values were tabulated and the percentage difference was recorded, using the hand calculation values as the base. Figure 54 shows the comparison between the hand calculations and the NTNU model.

Data Type	Parameters			Easy Conditions			Average Conditions			Hard Conditions		
	Name	Symbol	Unit	Hand Calculations	Excel Program	% Difference	Hand Calculations	Excel Program	% Difference	Hand Calculations	Excel Program	% Difference
Input	Cerchar abrasively index	CAI	/	3.4	3.4	/	3.67	3.67	/	4.1	4.1	/
Input	Brittleness value	S_20	%	49.5	49.5	/	39.9	39.9	/	27.16	27.16	/
Input	Sievers J value	S_j	1/10mm	20	20	/	9	9	/	1.74	1.74	/
Input	Tunnel length	L	m	5000	5000	/	5000	5000	/	5000	5000	/
Input	Weakness planes dip angle	α_f	°	75	75	/	75	75	/	75	75	/
Input	Joints direction (strike angle)	α_s	°	5	5	/	5	5	/	5	5	/
Input	Tunnel axis direction	α_t	°	15	15	/	15	15	/	15	15	/
Calculated	Tunnel axis-weakness plane angle	α	°	9.5	9.656	1.64	9.5	9.656	1.64	9.5	9.656	1.64
Calculated	Fracture class	FC	/	III-IV	III-IV	/	III-IV	III-IV	/	III-IV	III-IV	/
Calculated	Fracturing factor	k_s	/	1.85	1.869	1.03	1.85	1.869	1.03	1.85	1.869	1.03
Calculated	Drilling rate index	DRI	/	55	54.43	-1.04	40	43.4	8.50	20	29.716	48.58
Calculated	Drilling rate index factor	k_DRI	/	1.05	1.032	-1.71	0.9	0.96	6.67	0.75	0.846	12.80
Calculated	Equivalent factoring factor	k_eqv	/	1.94	1.582	-18.45	1.7	1.471	-13.47	1.4	1.297	-7.36
Calculated	Avg. gross thrust per cutter	M_b	kN/cutter	228.1	228	-0.04	228.1	228	-0.04	228.1	228	-0.04
Calculated	Cutter diameter factor	k_d	/	1.14	1.015	-10.96	1.14	1.015	-10.96	1.14	1.015	-10.96
Calculated	Cutter spacing factor	k_a	/	1.02	1.02	0.00	1.02	1.02	0.00	1.02	1.02	0.00
Calculated	Gross thrust per cutter	M_eqv	kN	265	236.097	-10.91	265	236.097	-10.91	265	236.097	-10.91
Calculated	Average cutter spacing	s	mm	64.5	64.52	0.03	64.5	64.52	0.03	64.5	64.52	0.03
Calculated	Critical thrust	M_1	kN	50	/	/	60	/	/	70	/	/
Calculated	Penetration exponent	b	/	1.3	/	/	1.4	/	/	1.5	/	/
Calculated	Basic penetration rate	i_0	mm/rev	10.33	6.255	-39.45	8	6.063	-24.21	7.4	5.742	-22.41
Input	Head rotation speed	v_rot	RPM	6	6	/	6	6	/	6	6	/
Calculated	Net penetration rate	I	m/hr	3.72	2.525	-32.12	2.88	2.183	-24.20	2.66	2.067	-22.29
Calculated	Cutter life index	CLI	/	7	25.4	262.86	7	21.25	203.57	7	15.45	120.71
Calculated	Basic cutter ring life	H_0	hr	42.5	95.578	124.89	42.5	89.9	111.53	42.5	73.829	73.72
Calculated	TBM correction factor	k_ ⌀	/	1.2	1.194	-0.50	1.2	1.194	-0.50	1.2	1.194	-0.50
Calculated	Quartz content	q	%	45%-85%	45%	/	45%-85%	45%	/	45%-85%	45	/
Calculated	Quartz content factor	k_Q	/	1	1.014	1.40	1	1.014	1.40	1	1.014	1.40
Calculated	Cutterhead rotation speed factor	k_RPM	/	2.08	2.083	0.14	2.08	2.083	0.14	2.08	2.083	0.14
Calculated	Number of TBM cutters	N_TBM	/	31	31	/	31	31	/	31	31	/
Calculated	Average number of cutters	N_0	#	30	29.735	-0.88	30	29.735	-0.88	30	29.735	-0.88
Calculated	Number of TBM cutters factor	k_N	#	1.03	1.043	1.26	1.03	1.043	1.26	1.03	1.043	1.26
Calculated	Cutter consumption	H_h	hr/cutter	3.52	8.282	135.28	3.52	7.63	116.76	3.52	6.266	78.01
Calculated	Cutter consumption	CRL	m3/cutter	164.46	234.36	42.50	127.33	209.275	64.36	117.6	162.778	38.42
Calculated	Net excavation time	T_net	Days	56	92.51	65.20	72.34	95.454	31.95	78.32	100.782	28.68
Calculated	Gross excavation time	T_gross	Days	112	185	65.18	144.68	190.908	31.95	156.64	201.563	28.68

Figure 54: Hand calculation values versus those of the NTNU model on the excel program

Figure 55 shows the comparison between the hand calculations and the CSM model.

Data Type	Parameters			Easy Conditions			Average Conditions			Hard Conditions		
	Name	Symbol	Unit	NTNU	CSM	% Difference	NTNU	CSM	% Difference	NTNU	CSM	% Difference
Calculated/Input	Basic penetration rate	i_0	mm/rev	6.255	18	187.77	6.063	18	196.88	5.742	18	213.48
Input	Net penetration rate (CSM)	I (CSM)	m/hr		6.48	156.63		6.48	196.84		6.48	213.50
Input	Net penetration rate (Js)	I (Js)	m/hr	2.525	3.708	46.85	2.183	3.708	69.86	2.067	3.708	79.39
Calculated	Net penetration rate	I	m/hr		/	/		/	/		/	/
Calculated	Cutter consumption	CRL	m3/cutter	234.36	392.093	67.30	209.275	363.247	73.57	162.778	325.15	99.75
Calculated	Net excavation time (CSM)	T_net	Days		32.15	-65.25		32.15	-66.32		32.15	-68.10
Calculated	Net excavation time (Js)	T_net	Days	92.51	56.187	-39.26	95.454	56.187	-41.14	100.782	56.187	-44.25
Calculated	Net excavation time	T_net	Days		/	/			/			/
Calculated	Gross excavation time (CSM)	T_gross	Days		64.3	-65.24		64.3	-66.32		64.3	-68.10
Calculated	Gross excavation time (Js)	T_gross	Days	185	112.375	-39.26	190.908	112.35	-41.15	201.563	112.35	-44.26
Calculated	Gross excavation time	T_gross	Days		/	/		/	/		/	/

Figure 55: Hand calculation values versus those of the CSM model on the excel program

Figure 56 shows the comparison between the NTNU and the CSM models.

Data Type	Parameters			Easy Conditions			Average Conditions			Hard Conditions		
	Name	Symbol	Unit	Hand Calculations	Excel Program	% Difference	Hand Calculations	Excel Program	% Difference	Hand Calculations	Excel Program	% Difference
Input	Cerchar abrasively index	CAI	/	3.4	3.4	/	3.67	3.67	/	4.1	4.1	/
Input	Brittleness value	S_20	%	49.5	49.5	/	39.9	39.9	/	27.16	27.16	/
Input	Sievers J value	S_j	1/10mm	20	20	/	9	9	/	1.74	1.74	/
Input	Tunnel length	L	m	5000	5000	/	5000	5000	/	5000	5000	/
Input	Weakness planes dip angle	α_f	°	75	75	/	75	75	/	75	75	/
Input	Joints direction (strike angle)	α_s	°	5	5	/	5	5	/	5	5	/
Input	Tunnel axis direction	α_t	°	15	15	/	15	15	/	15	15	/
Calculated	Tunnel axis-weakness plane angle	α	°	9.5	9.656	1.64	9.5	9.656	1.64	9.5	9.656	1.64
Calculated	Fracture class	FC	/	III-IV	III-IV	/	III-IV	III-IV	/	III-IV	III-IV	/
Calculated/Input	Basic penetration rate	i_0	mm/rev	10.33	18	74.25	8	18	125.00	7.4	18	143.24
Input	Head rotation speed	v_rot	RPM	6	6	/	6	6	/	6	6	/
Input	Net penetration rate (CSM)	I (CSM)	m/hr		6.48	74.19		6.48	125.00		6.48	143.61
Input	Net penetration rate (Js)	I (Js)	m/hr	3.72	3.708	-0.32	2.88	3.708	28.75	2.66	3.708	39.40
Calculated	Net penetration rate	I	m/hr		/	/		/	/		/	/
Calculated	Cutter consumption	CRL	m3/cutter	164.46	392.093	138.41	127.33	363.247	185.28	117.6	325.15	176.49
Calculated	Net excavation time (CSM)	T_net	Days		32.15	-42.59		32.15	-55.56		32.15	-58.95
Calculated	Net excavation time (Js)	T_net	Days	56	56.187	0.33	72.34	56.187	-22.33	78.32	56.187	-28.26
Calculated	Net excavation time	T_net	Days		/	/		/	/		/	/
Calculated	Gross excavation time (CSM)	T_gross	Days		64.3	-42.59		64.3	-55.56		64.3	-58.95
Calculated	Gross excavation time (Js)	T_gross	Days	112	112.375	0.33	144.68	112.35	-22.35	156.64	112.35	-28.28
Calculated	Gross excavation time	T_gross	Days		/	/		/	/		/	/

Figure 56: NTNU versus CSM values

Other models were also considered and implemented into the program to produce their own respective set of output values. Most of these equations used less overall input data directly related to rock and TBM parameters, but instead use general codes and weighted values. In light of this, they may not be able to represent all the data comparable with the larger CSM and NTNU models, but nonetheless they were included to broaden the range of possible output values.

6. Comments

A percentage difference was implemented as it was deemed the best way to show any differences between the hand calculation and prediction model values. For ease of reference, increases were marked in green, and decreases were marked in red.

From the tabulated data, it can be understood that there seems to be an even split between drastically different changes, and almost negligible changes. The percentage differences were compared side by side, and it was interesting to note that difference was not constant between some parameters for the easy, average, and hard conditions.

Various reasons may exist as to why one value differs greatly from the other and it was attempted to logically explain these differences as best as possible. In most cases, the each output value difference was investigated by analysing the fundamental equations and parameters involved to produce that output, essentially working backwards and identifying the influential variables, if any.

It is also important to note that for the CSM prediction model, the maximum penetration rate was found before the normal force exceeds the max allowable force of the cutters. This is an important metric as it not only enables the discs to work at peak efficiency, but also ensures that they are not over-worn for the amount of penetration they create. Furthermore, the risk of the discs completely breaking and being unusable right away is greatly reduced. Through the analysis, it was established that the maximum penetration is 18 mm, much greater than that of in the NTNU model but also the same as in the hand calculations.

Tables 9 and 10 show the percentage difference side by side for all the conditions and the potential reasons as to why there is a difference.

Hand calculations vs NTNU model differences:

Name and Parameter		Easy	Average	Hard	Potential reason
Tunnel axis-weakness plane angle	α	1.64	1.64	1.64	Rounding erros
Fracturing factor	k_s	1.03	1.03	1.03	Graphical errors vs numerical values through equations
Drilling rate index	DRI	-1.04	8.50	48.58	Graphical errors vs numerical values through equations
Drilling rate index factor	k_DRI	-1.71	6.67	12.80	Graphical errors vs numerical values through equations
Equivalent factoring factor	k_eqv	-18.45	-13.47	-7.36	Differences based on previously calculated independent variables
Avg. gross thrust per cutter	M_b	-0.04	-0.04	-0.04	Rounding erros
Cutter diameter factor	k_d	-10.96	-10.96	-10.96	Graphical errors vs numerical values through equations
Cutter spacing factor	k_a	0.00	0.00	0.00	-
Gross thrust per cutter	M_eqv	-10.91	-10.91	-10.91	Differences based on previously calculated independent variables
Average cutter spacing	s	0.03	0.03	0.03	Rounding erros
Basic penetration rate	i_0	-39.45	-24.21	-22.41	Program uses equations based on k_{ekv} instead of critical thrust and exponent coefficients.
Net penetration rate	I	-32.12	-24.20	-22.29	Due to difference in i_0
Cutter life index	CLI	262.86	203.57	120.71	Graphical error vs standard equation
Basic cutter ring life	H_0	124.89	111.53	73.72	Graphical error and CLI difference
TBM correction factor	k_ ⌀	-0.50	-0.50	-0.50	Graphical errors vs numerical values through equations
Quartz content factor	k_Q	1.40	1.40	1.40	Graphical errors vs numerical values through equations
Cutterhead rotation speed factor	k_RPM	0.14	0.14	0.14	Rounding erros
Average number of cutters	N_0	-0.88	-0.88	-0.88	Graphical errors vs numerical values through equations
Number of TBM cutters factor	k_N	1.26	1.26	1.26	Differences based on previously calculated independent variables
Cutter consumption	H_h	135.28	116.76	78.01	Differences based on previously calculated independent variables
Cutter consumption	CRL	42.50	64.36	38.42	Differences based on previously calculated independent variables
Net excavation time	T_net	65.20	31.95	28.68	Differences based on previously calculated independent variables
Gross excavation time	T_gross	65.18	31.95	28.68	Differences based on previously calculated independent variables

Table 9: Hand calculations vs NTNU model percentage differences

Hand calculations vs CSM model differences:

Name and Parameter		Easy	Average	Hard	Potential reason
Tunnel axis-weakness plane angle	α	1.64	1.64	1.64	Rounding erros
Basic penetration rate	i_0	74.25	125.00	143.24	Program uses equations based on max cutter force instead of critical thrust and exponent coefficients.
Net penetration rate (CSM)	I (CSM)	74.19	125.00	143.61	Due to difference in i_0
Net penetration rate (Js)	I (Js)	-0.32	28.75	39.40	Due to difference in i_0 and correction factors
Cutter consumption	CRL	138.41	185.28	176.49	Differences based on previously calculated independent variables
Net excavation time (CSM)	T_net	-42.59	-55.56	-58.95	Differences based on previously calculated independent variables
Net excavation time (Js)	T_net	0.33	-22.33	-28.26	Differences based on previously calculated independent variables
Gross excavation time (CSM)	T_gross	-42.59	-55.56	-58.95	Differences based on previously calculated independent variables
Gross excavation time (Js)	T_gross	0.33	-22.35	-28.28	Differences based on previously calculated independent variables

Table 10: Hand calculations vs CSM model percentage differences

7. Conclusions

The different prediction models utilise their own input variables, and all directly present a set of outputs which can be compared side by side to obtain a better understanding of the TBM's cutter performance. Of course, as these individual methods rely on different input data and processing functions, differences in values will emerge. Isolated, the prediction values have no context to be compared with, but when looking at all the available inputs and outputs together, a range of predictions for the wear and performance of the cutters will be obtained. More credibility can be placed on the final values if they resemble one another and match those from field data as the prediction is there to estimate what actually happens to the cutters when used.

The output data was within a close range of results, for instance, the net penetration rate for the NTNU and CSM models in hard conditions were 2.067 m/hr and 3.708 m/hr respectively. Based on the available literature and real life examples, these are within an expected range of values.

Other values were also compared and revealed greater differences such as in the cutter ring life expressed in m^3/cutter. This is to be expected with one reason being that the CSM model will have a higher penetration rate since it is based on the maximum force applied onto the cutter, rather than accounting for rock variability like in the NTNU model.

A key point to keep in mind is that some differences arise due to the use of more precise equations over hand calculations and graphical value selection. The margin of error increases when working via the hand calculations and taking values directly from graphs, and this is mitigated through the equations.

As the input data spans a wide range of variables, inconsistencies exist. To combat this, a larger set of input data will need to be obtained from existing projects and homogenised to ensure that the inputs being used for the calculations have some relation to one another. This may close the gap between the values of the different methods and increase the certainty of the results. To this end, the output data is within expected values, but many more input datasets will be required to build a larger and more reliable set of output values that fall within a smaller range and therefor there will be more confidence in the prediction results.

In conclusion, while the output values are within a broad expected range, improvements can come about through the growth and standardisation of the data sets used. This will involve obtaining more data and organising it such that variables can be directly linked together, for example through their own natural properties. More iterations will then be made to build a substantial output database from which more certainty can be derived from the emerging patterns. Comparing these output values with actual past project data will validate their degree of precision. Results can also then be used to help determine the precision of hand calculations and graphical methods.

8. Bibliography

A. Bruland (2000), Hard Rock Tunnel Boring Vol. 8 - Drillability - Test Methods. http://dx.doi.org/10.13140/RG.2.1.3363.4729

A. Bruland (1998) Hard rock tunnel boring, NTNU Trondheim Norwegian University of Sciences and Technology, PhD thesis

E. Farrokh, J Rostami, C. Laughton (2012), Study of various models for estimation of penetration rate of hard rock TBMs. https://doi.org/10.1016/j.tust.2012.02.012

F. Dahl, A. Bruland, P. D. Jakobsen, B. Nilsen, E. Grøv (2011), Classifications of properties influencing the drillability of rocks, based on the NTNU/SINTEF test method. Tunnelling and Underground Space Technology, Volume 28. https://doi.org/10.1016/j.tust.2011.10.006

H. Zhang, M. Xia, F. Huang, Z. Zhang (2024), Research on Rock-Breaking Characteristics of Cutters and Matching of Cutter Spacing and Penetration for Tunnel Boring Machine. https://doi.org/10.3390/buildings14061757

J. Hassanpour, J. Rostami, J. Zhao (2011), A new hard rock TBM performance prediction model for project planning. https://doi.org/10.1016/j.tust.2011.04.004

J. Rostami (2016), Performance prediction of hard rock Tunnel Boring Machines (TBMs) in difficult ground. Tunnelling and Underground Space Technology, Volume 57. https://doi.org/10.1016/j.tust.2016.01.009

J. Rostami, L. Ozdemir (1993), New model for performance production of hard rock TBMs. https://www.researchgate.net/publication/288383954_New_model_for_performance_production_of_hard_rock_TBMs

K. There, H. Käsling (2011), Grundlagen der Penetrations- und Verschleißprognose beim TBM-Vortrieb im Fels. https://ethz.ch/content/dam/ethz/special-interest/baug/igt/tunneling-dam/kolloquien/2011/thuro_grundlagen.pdf

L. Jing, J. Li, N. Zhang, S. Chen, C. Yang, H. Cao (2021), A TBM advance rate prediction method considering the effects of operating factors. Tunnelling and Underground Space Technology, Volume 107. https://doi.org/10.1016/j.tust.2020.103620

M. Alber (1996), Prediction of Penetration And Utilization For Hard Rock TBMs

M. A. Grima, P. A. Bruines, P. N. W. Verhoef (2000), Modeling tunnel boring machine performance by neuro-fuzzy methods. Tunnelling and Underground Space Technology, Volume 15. https://doi.org/10.1016/S0886-7798(00)00055-9

M. Cardu, E. Catanzaro, A. Farinetti, D. Martinelli, C. Todaro (2021), Performance Analysis of Tunnel Boring Machines for Rock Excavation. https://doi.org/10.3390/app11062794

P. Grasso, A. Lavagno, G. Brino Geodata, M. Cardu, D. Martinelli, C. Todaro, A. Carigi, G. Cotugno, D. Peila, M. Concilia, S. Bechter, M. Bringiotti, D. Nicastro, V. Manassero, T. Peinsitt, S. Santarelli (2023), Volume 2 of Handbook on Tunnels and Underground Works.

P. Jain, A. K. Naithani, T. N. Singh (2015), Performance Characteristics of Tunnel Boring Machines and Correlation with Empirical Prediction Model - Case Study From Mumbai, India. https://www.researchgate.net/publication/283352613_Performance_Characteristics_of_Tunnel_Boring_Machines_and_Correlation_with_Empirical_Prediction_Model_-_Case_Study_From_Mumbai_India

Q. M. Gong, J. Zhao (2009), Development of a rock mass characteristics model for TBM penetration rate prediction. https://doi.org/10.1016/j.ijrmms.2008.03.003

S. W. Lee, S. H. Chang, K. H. Park, C. Y. Kim (2011), TBM Performance and Development State in Korea. http://dx.doi.org/10.1016/j.proeng.2011.07.400

S. Yagiz (2008), Utilizing rock mass properties for predicting TBM performance in hard rock condition. Tunnelling and Underground Space Technology, Volume 23. https://doi.org/10.1016/j.tust.2007.04.011